

1 **Transposable elements regulate thymus development and function**

2 **Authors**

3 Jean-David Larouche^{1,2}, Céline M. Laumont^{3,4}, Assya Trofimov^{1,5,6,7}, Krystel Vincent¹, Leslie Hesnard¹,
4 Sylvie Brochu¹, Caroline Côté¹, Juliette Humeau¹, Éric Bonneil¹, Joël Lanoix¹, Chantal Durette¹, Patrick
5 Gendron¹, Jean-Philippe Laverdure¹, Ellen R. Richie⁸, Sébastien Lemieux^{1,9}, Pierre Thibault^{1,10}, Claude
6 Perreault^{1,2*}.

7

8 **Affiliations**

9 ¹ Institute for Research in Immunology and Cancer, Université de Montréal; Montréal, Canada.

10 ² Department of Medicine, Université de Montréal; Montréal, Canada.

11 ³ Deeley Research Centre, BC Cancer; Victoria, Canada.

12 ⁴ Department of Medical Genetics, University of British Columbia; Vancouver, Canada.

13 ⁵ Department of Computer Science and Operations Research, Université de Montréal; Montréal, Canada.

14 ⁶ Department of Physics, University of Washington; Seattle, USA.

15 ⁷ Fred Hutchinson Cancer Center; Seattle, USA.

16 ⁸ Department of Epigenetics and Molecular Carcinogenesis, University of Texas M.D. Anderson Cancer
17 Center; Houston, USA.

18 ⁹ Department of Biochemistry and Molecular Medicine, Université de Montréal; Montréal, Canada.

19 ¹⁰ Department of Chemistry, Université de Montréal; Montréal, Canada.

20 *Corresponding author. Email: claude.perreault@umontreal.ca

21 **Abstract**

22 Transposable elements (TE) are repetitive sequences representing ~45% of the human and mouse
23 genomes and are highly expressed by medullary thymic epithelial cells (mTEC). In this study, we
24 investigated the role of TEs on T-cell development in the thymus. We performed multi-omic analyses of
25 TEs in human and mouse thymic cells to elucidate their role in T cell development. We report that TE
26 expression in the human thymus is high and shows extensive age- and cell lineage-related variations. TE
27 expression correlates with multiple transcription factors in all cell types of the human thymus. Two cell
28 types express particularly broad TE repertoires: mTECs and plasmacytoid dendritic cells (pDC). In
29 mTECs, transcriptomic data suggest that TEs interact with transcription factors essential for mTEC
30 development and function (e.g., PAX1 and REL), and immunopeptidomic data showed that TEs
31 generate MHC-I-associated peptides implicated in thymocyte education. Notably, AIRE, FEZF2, and
32 CHD4 regulate small yet non-redundant sets of TEs in murine mTECs. Human thymic pDCs
33 homogenously express large numbers of TEs that likely form dsRNA, which can activate innate immune
34 receptors, potentially explaining why thymic pDCs constitutively secrete IFN α/β . This study highlights
35 the diversity of interactions between TEs and the adaptive immune system. TEs are genetic parasites,
36 and the two thymic cell types most affected by TEs (mTECs and pDCs) are essential to establishing
37 central T-cell tolerance. Therefore, we propose that orchestrating TE expression in thymic cells is
38 critical to prevent autoimmunity in vertebrates.

39

40

41 **Introduction**

42 Self/non-self discrimination is a fundamental requirement of life (1). In jawed vertebrates, the thymus is
43 the only site where T lymphocytes can be properly educated to distinguish self from non-self (2, 3). This
44 is vividly illustrated by Oncostatin M-transgenic mice, where T-cell production occurs exclusively in the
45 lymph nodes (4). These mice harbor normal numbers of T-cell receptors (TCR) $\alpha\beta$ T cells but present
46 severe autoimmunity and cannot fight infections (5). Intrathymic generation of a functional T-cell
47 repertoire depends on choreographed interactions between the TCRs of thymocytes and peptides
48 presented by major histocompatibility complex (MHC) molecules on various antigen-presenting cells
49 (APC) (6). Positive selection depends on self-antigens presented by cortical thymic epithelial cells
50 (cTEC) and ensures that TCRs recognize antigens in the context of the host's MHC molecules (7, 8).
51 The establishment of central tolerance depends on two main classes of APCs located in the thymic
52 medulla: dendritic cells (DC) and medullary TEC (mTEC) (9-11). Two other APC types have a more
53 limited contribution to central tolerance: thymic fibroblasts and B cells (12, 13). High avidity
54 interactions between thymic APCs and autoreactive thymocytes lead to thymocyte deletion (negative
55 selection) or generation of regulatory T cells (Treg) (14).

56

57 The main drivers of central tolerance, mTECs and DCs, display considerable phenotypic and functional
58 heterogeneity. Indeed, recent single-cell RNA-seq (scRNA-seq) studies have identified several
59 subpopulations of mTECs: immature mTEC(I) that stimulate thymocyte migration to the medulla via
60 chemokine secretion (15), mTEC(II) that express high levels of MHC and are essential to tolerance
61 induction, fully differentiated corneocyte-like mTEC(III) that foster a pro-inflammatory
62 microenvironment (16), and finally mimetic mTECs that express peripheral tissue antigens (17). Three
63 different proteins whose loss of function leads to severe autoimmunity, AIRE, FEZF2, and CHD4, have

64 been shown to drive the expression of non-redundant sets of peripheral tissue antigens in mTECs (18-
65 20). DCs, on the other hand, are separated into three main populations. Conventional DC 1 and 2 (cDC1
66 and cDC2) have an unmatched ability to present both endogenous antigens and exogenous antigens
67 acquired via cross-presentation or cross-dressing (21). Plasmacytoid DC (pDC) are less effective APCs
68 than cDCs, their primary role being to produce interferon alpha (IFN \square) (21). Notably, thymic pDCs
69 originate from intrathymic IRF8^{hi} precursors, and, in contrast to extrathymic pDCs, they constitutively
70 secrete high amounts of IFN \square (22-24). This constitutive IFN \square secretion by thymic pDCs regulates the
71 late stages of thymocyte development by promoting the generation of Tregs and innate CD8 T cells (25-
72 29).

73

74 Transposable elements (TE) are repetitive sequences representing ~45% of the human and mouse
75 genomes (30, 31). Most TEs can be grouped into three categories: the long and short interspersed
76 nuclear elements (LINE and SINE, respectively) and the long terminal repeats (LTR). These broad
77 categories are subdivided into over 800 subfamilies based on sequence homology (32). TE expression is
78 typically repressed in host cells to prevent deleterious integrations of TE sequences in protein-coding
79 genes (33). Unexpectedly, TEs were recently found to be expressed at higher levels in human mTECs
80 than in any other MHC-expressing tissues and organs (i.e., excluding the testis) (34, 35), suggesting a
81 role for TEs in thymopoiesis. Since some TEs are translated and generate MHC I-associated peptides
82 (MAP) (34), they might induce TE-specific central tolerance (36). Additionally, TEs provide binding
83 sites to transcription factors (TF) and stimulate cytokine secretion via the formation of double-stranded
84 RNA (dsRNA) (37-41). Hence, TEs could have pleiotropic effects on thymopoiesis. To evaluate the role
85 of TEs in thymopoiesis, we adopted a multipronged strategy beginning with scRNA-seq of human thymi
86 and culminating in MS analyses of the MAP repertoire of mouse mTECs.

87

88 **Results**

89 **LINE, LTR, and SINE expression shows extensive variations during ontogeny of the human**
90 **thymus**

91 We first profiled TE expression in various thymic cell populations during development. To do so, we
92 quantified the expression of 809 TE subfamilies (classified according to the RepeatMasker annotations)
93 in the scRNA-seq dataset of human thymi created by *Park et al.* (42). Cells were clustered in 19
94 populations representing the main constituents of the thymic hematolymphoid and stromal
95 compartments (Figure 1a and Figure 1 – figure supplement 1). The expression of TE subfamilies was
96 quantified at all developmental stages available, ranging from 7 post-conception weeks (pcw) to 40
97 years of age (Supplementary file 1 – Table 1). Unsupervised hierarchical clustering revealed three
98 clusters of TE subfamilies based on their pattern of expression during thymic development (Figure 1b,
99 upper panel): i) maximal expression at early embryonic stages persisting, albeit at lower levels,
100 throughout ontogeny (cluster 1), ii) an expression specific to a given timepoint (cluster 2), or iii) a high
101 expression at early embryonic stages that decreases rapidly at later timepoints (cluster 3). LINE and
102 SINE subfamilies were enriched in cluster 1, whereas LTR subfamilies were significantly enriched in
103 clusters 2 and 3 (Figure 1b, lower panel). Expression of individual LINE and SINE subfamilies was
104 highly shared among different cell types (Figure 1d). In contrast, the LTR subfamilies' expression
105 pattern was shared by fewer cell subsets and adopted a quasi-random distribution (Figure 1d). The
106 pattern of expression assigned to TE subfamilies (Figure 1c, innermost track) was not affected by the
107 proportion of cells of different developmental stages (embryonic or postnatal) (Figure 1c, outermost
108 track, and Figure 1 – figure supplement 2). This suggests that our observations do not result from a bias
109 in the composition of the dataset. To gain further insights into the expression of TE subfamilies, we

110 studied two biological processes known to regulate TE expression in other contexts: cell proliferation
111 and expression of KRAB zinc-finger proteins (KZFP) (43, 44). Cell cycling scores negatively correlated
112 with TE expression in various thymic cell subsets, particularly for LINE and SINE subfamilies shared
113 among cell types (Figure 1 – figure supplement 3 and Supplementary file 1 – Table 2), whereas analysis
114 of KZFP expression identified ZNF10 as a probable repressor of L1 subfamilies in Th17 and NK cells
115 (Figure 1 – figure supplement 4 and Supplementary file 1 – Table 3). Thus, we conclude that the
116 expression of the three main classes of TEs shows major divergences as a function of age and thymic
117 cell types.

118

119 **TEs form interactions with transcription factors regulating thymic development and function**

120 TEs provide binding sites to TFs (37, 45, 46), and T-cell development is driven by the coordinated
121 timing of multiple changes in transcriptional regulators (47). We, therefore, investigated interactions
122 between TE subfamilies and TFs during the development of the human thymus. Two criteria defined an
123 interaction: i) a significant and positive correlation between the expression of a TF and a TE subfamily
124 in a given cell population, and ii) the presence of the TF binding motif in the loci of the TE subfamily
125 (Figure 2a). Additionally, we validated the correlations we obtained using a bootstrap procedure to
126 ascertain their reproducibility (see *Material and Methods* for details). This procedure removed weakly
127 correlated TF-TE pairs (Figure 2b). TF-TE interactions were observed in all thymic cell populations
128 (Figure 2c, d, Figure 2 – figure supplement 1, and Supplementary file 1 – Table 4). Numerous TF-TE
129 interactions were conserved between hematolymphoid and stromal cell subsets (Figure 2e). However,
130 the number of interactions and the complexity of the interaction networks were much higher in mTECs
131 than in other cell populations (Figure 2c, d, Figure 2 – figure supplement 1, and Figure 2 – figure
132 supplement 2).

133

134 Several TFs instrumental in thymus development and thymopoiesis interacted with TE subfamilies
135 (Figure 2 – figure supplement 2, and Supplementary file 1 – Table 4). These TFs include the *NFKB1* and
136 *REL* subunits of the NF- κ B complex and *PAX1* in mTECs (48-50) and *JUND* in thymocytes (51). In
137 DCs, the most notable TF-TE interactions involved interferon regulatory factors (IRF), which regulate
138 the late stages of T-cell maturation, and *TCF4*, which is essential for pDC development (25, 52). This
139 observation is consistent with evidence that TEs have shaped the evolution of IFN signaling networks
140 (37). Finally, we found significant interactions between *CTCF* and TE subfamilies in mTECs and
141 endothelial cells, suggesting that the binding of *CTCF* to TE sequences affects the tridimensional
142 structure of the chromatin in the thymic stroma (53). Interestingly, LINE and SINE subfamilies that
143 occupy more genomic space interacted with higher numbers of transcription factors (Figure 2 – figure
144 supplement 3).

145

146 Using data from the ENCODE consortium for hematopoietic cells (54, 55), we looked at the histone
147 marks at the TE loci identified as TF interactors by our analyses (i.e., correlated with TF expression and
148 containing the TF binding motif). The objective was to determine if they could act as promoters or
149 enhancers (Figure 2a and Supplementary file 1 – Table 5). We found several TE promoter and enhancer
150 candidates in all eight hematopoietic cell types analyzed, with a striking overrepresentation of LINE and
151 SINE compared to LTR sequences (Figure 2f and Supplementary file 1 – Table 6). Finally, we analyzed
152 publicly available ChIP-seq data of ETS1, an important TF for NK cell development (56), to confirm its
153 ability to bind TE sequences. Indeed, 19% of ETS1 peaks overlap with TE sequences (Figure 2g).
154 Notably, ETS1 peaks overlapped with TE sequences (Figure 2h, in red) in the promoter regions of PRF1

155 and KLRD1, two genes critical for NK cells' effector functions (57, 58). Hence, our data suggest that
156 TEs affect thymic development and function by providing binding sites to multiple TFs.

157

158 **TEs are highly and differentially expressed in human thymic APC subsets**

159 We next sought to determine whether the high expression of TEs reported in mTECs (32, 33) was
160 limited to this cell subset or was found in other thymic cell types. Since several thymic stromal cells
161 reach maturity after birth (59), we selected postnatal samples for the following analyses. We computed
162 two distinct Shannon entropy indices: one for the global diversity of TEs expressed by all cells of a
163 given population, and another for the median value of TE diversity expressed by individual cells of a
164 population (Figure 3a). Then, we computed a linear model to represent the diversity of TEs expressed by
165 a cell population based on the diversity of TEs expressed by individual cells (Figure 3a, blue curve).
166 Two salient findings emerged from this analysis. First, the diversity of TEs expressed in the T-cell
167 lineage decreases during differentiation according to the following hierarchy: DN thymocytes > DP
168 thymocytes > SP thymocytes (Figure 3a, Figure 3 – figure supplement 1). Second, among the
169 populations of thymic APCs implicated in positive and negative selection (Figure 3a, orange dots),
170 cTECs, mTECs, and DCs expressed broader repertoires of TEs than B cells and fibroblasts. While
171 cTECs and DCs expressed highly diverse TE repertoires at both the population and individual cell
172 levels, the breadth of TE expression in mTECs was found only at the population level (Figure 3a).
173 Accordingly, intercellular heterogeneity (i.e., deviation from the linear model) was higher for mTECs
174 than other cell populations (Figure 3b).

175

176 We next focused on thymic APCs expressing the broadest TE repertoires: cTECs, mTECs, and DCs
177 (Figure 3a). To this end, we annotated these APC subpopulations based on previously published lists of
178 marker genes (Figure 3c and Figure 3 – figure supplement 2) (42, 60). We performed differential
179 expression analyses to determine whether some TE subfamilies were overexpressed in specific APC
180 subsets. pDCs and mTEC(II) overexpressed a broader TE repertoire than other APCs: 32.01% of
181 subfamilies were overexpressed in pDCs and 10.88% in mTEC(II) (Figure 3d and Supplementary file 1
182 – Table 7). The nature of the overexpressed TEs differed between pDCs and other thymic APC subsets.
183 Indeed, pDCs overexpressed LTRs, LINEs, and SINEs, including several Alu and L1 subfamilies
184 (Figure 3d and Supplementary file 1 – Table 7). In contrast, other thymic APCs predominantly
185 overexpressed LTRs.

186

187 TE expression showed wildly divergent levels of intercellular heterogeneity in APC subsets. Indeed,
188 whereas most TE subfamilies were expressed by <25% of cells of the mTEC(II) population, an
189 important proportion of TEs were expressed by >75% of pDCs (Figure 3e). To evaluate this question
190 further, we compared TE expression between metacells of thymic APCs; metacells are small clusters of
191 cells with highly similar transcription profiles. This analysis revealed that overexpression of TE
192 subfamilies was shared between pDC metacells but not mTEC(II) metacells, reinforcing the idea that TE
193 expression adopts a mosaic pattern in the mTEC(II) population (Figure 3 – figure supplement 3). We
194 conclude that cTECs, mTECs, and DCs express broad TE repertoires. However, two subpopulations of
195 thymic APCs clearly stand out. pDCs express an extremely diversified repertoire of LTRs, SINEs, and
196 LINEs, showing limited intercellular heterogeneity, whereas the mTEC(II) population shows a highly
197 heterogeneous overexpression of LTR subfamilies.

198

199 **TE expression in human pDCs is associated with dsRNA structures**

200 The high expression of a broad repertoire of TE sequences in thymic pDCs was unexpected (Figure 3d).
201 LINE and SINE subfamilies, in particular, were highly and homogeneously expressed by thymic pDCs
202 (Figure 4a). Constitutive IFN α secretion is a feature of thymic pDCs not found in extrathymic pDCs.
203 We, therefore, hypothesized that this constitutive IFN α secretion by thymic pDCs might be
204 mechanistically linked to their TE expression profile. We first assessed whether thymic and extrathymic
205 pDCs have similar TE expression profiles by reanalyzing scRNA-seq data from human spleens
206 published by *Madissoon et al.* (61) (Figure 4 – figure supplement 1a, b). This revealed that extrathymic
207 pDCs express TE sequences at similar or lower levels than other splenic cells (Figure 4 – figure
208 supplement 1c, d). We then used pseudobulk RNA-seq methods to perform a differential expression
209 analysis of TE subfamilies between thymic and splenic pDCs. This analysis confirmed that TE
210 expression was globally higher in thymic than in extrathymic pDCs (Figure 4b). Since TE
211 overexpression can lead to the formation of dsRNA (40, 41), we investigated if such structures were
212 found in thymic pDCs. pDCs were magnetically enriched from primary human thymi following labeling
213 with anti-CD303 antibody (a marker of pDCs). Then, pDC-enriched thymic cells were stained with an
214 antibody against CD123 (another marker of pDCs) and the J2 antibody that stains dsRNA. The intensity
215 of the J2 signal was more than 10-fold higher in CD123 $^{+}$ relative to CD123 $^{-}$ cells (Figure 4c, d). We
216 conclude that thymic pDCs contain large amounts of dsRNAs. To evaluate if these dsRNAs arise from
217 TE sequences, we analyzed in thymic APC subsets the proportion of the transcriptome assigned to two
218 groups of genomic sequences known as important sources of dsRNAs: TEs and mitochondrial genes
219 (62). Strikingly, whereas the percentage of reads from mitochondrial genes was typically lower in pDCs
220 than in other thymic APCs, the proportion of the transcriptome originating from TEs was higher in
221 pDCs (~22%) by several orders of magnitude (Figure 4 – figure supplement 2). Finally, we performed

222 gene set enrichment analyses to ascertain if the high expression of TEs by thymic pDCs was associated
223 with specific gene signatures. These analyses highlighted signatures of antigen presentation, immune
224 response, and interferon signaling in thymic pDCs (Figure 4e and Supplementary file 1 – Table 8).
225 Notably, thymic pDCs harbored moderate yet significant enrichment of gene signatures of RIG-I and
226 MDA5-mediated IFN α/β signaling compared to all other thymic APCs (Figure 4e and Supplementary
227 file 1 – Table 8). Altogether, these data support a model in which the high and ubiquitous expression of
228 TEs in thymic pDCs would lead to the formation of dsRNAs triggering innate immune sensors, which
229 might explain their constitutive secretion of IFN α/β .

230

231 **AIRE, CHD4, and FEZF2 regulate distinct sets of TE sequences in murine mTECs**

232 The essential role of mTECs in central tolerance hinges on their ability to ectopically express tissue-
233 restricted genes, whose expression is otherwise limited to specific epithelial lineage (63, 64). This
234 promiscuous gene expression is driven by AIRE, CHD4, and FEZF2 (18-20). We, therefore,
235 investigated the contribution of these three genes to the expression of TE subfamilies in the mTEC(II)
236 population (Figure 3d). First, we validated that mTEC(II) express *AIRE*, *CHD4*, and *FEZF2* in the
237 human scRNA-seq dataset (Figure 5a). Next, we analyzed published murine mTEC RNA-seq data to
238 assess the regulation of TE sequences by AIRE, CHD4, and FEZF2. Differential expression analyses
239 between knock-out (KO) and wild-type (WT) mice showed that these three factors regulate TE
240 sequences, but the magnitude and directionality of this regulation differed (Figure 5b and Supplementary
241 file 1 – Table 9). Indeed, while CHD4 had the biggest impact on TE expression by inducing 433 TE loci
242 and repressing 463, FEZF2's impact was minimal, with 97 TE loci induced and 60 repressed (Figure
243 5b). Besides, AIRE mainly acted as a repressor of TE sequences, with 326 loci repressed and 171
244 induced (Figure 5b). Interestingly, there was minimal overlap between the TE sequences regulated by

245 AIRE, CHD4, and FEZF2, indicating that they have non-redundant roles in TE regulation (Figure 5c).
246 Additionally, AIRE, CHD4, and FEZF2 preferentially targeted LTR and LINE elements, with
247 significant enrichment of specific subfamilies such as MTA_Mm-int and RLTR4_Mm that are induced
248 by Aire and Fezf2, respectively (Figure 5d and Figure 5 – figure supplement 1a). While AIRE and
249 CHD4 preferentially targeted evolutionary young TE sequences, the age of the TE sequence did not
250 seem to affect the regulation by FEZF2 (Figure 5 – figure supplement 1b). We also noticed that the
251 distance between regulated TE loci was smaller than the distributions of randomly selected TEs (Figure
252 5 – figure supplement 1c). This suggests that AIRE, CHD4, and FEZF2 nonrandomly affect the
253 expression of TE sequences located in specific genomic regions. We observed no significant differences
254 in the genomic localization of TE loci targeted by AIRE, CHD4, and FEZF2 relative to the genomic
255 localization of all TE sequences in the murine genome: most TE loci were located in intronic and
256 intergenic regions (Figure 5 – figure supplement 1d). Enrichment for intronic TEs could not be ascribed
257 to induction of global intron retention: the intron retention ratio was similar for TEs regulated or not by
258 AIRE, CHD4, and FEZF2 (Figure 5 – figure supplement 1e). ChIP-seq-based analysis of permissive
259 histone marks showed that TE loci induced by AIRE, CHD4, and FEZF2 were all marked by H3K4me3
260 (Figure 5e). As a proof of concept, we validated that 31.42% of AIRE peaks overlap with TE sequences
261 by reanalyzing ChIP-seq data, confirming AIRE’s potential to bind TE sequences (Figure 5f). Hence,
262 AIRE, CHD4, and FEZF2 regulate the expression of small yet non-redundant repertoires of TE
263 sequences associated with permissive histone marks.

264

265 **TEs are translated and presented by MHC class I molecules in murine TECs**

266 Several TEs are translated and generate MAPs (34). Hence, the expression of TEs in cTECs and even
267 more in mTECs raises a fundamental question: do these TEs generate MAPs that would shape the T cell

268 repertoire? Mass spectrometry (MS) is the only method that can faithfully identify MAPs (65-67).
269 Despite its quintessential role in central tolerance, the MAP repertoire of mTECs has never been studied
270 by MS because of the impossibility of obtaining sufficient mTECs for MS analyses: mTECs represent \leq
271 1% of thymic cells, and they do not proliferate *in vitro*. To get enough cTECs and mTECs for MS
272 analyses, we used transgenic mice that express cyclin D1 under the control of the keratin 5 promoter
273 (K5D1 mice). These mice develop dramatic thymic hyperplasia, but their thymus is morphologically and
274 functionally normal (68-70). Primary cTECs and mTECs (2 replicates of 70×10^6 cells from 121 and 90
275 mice, respectively) were isolated from the thymi of K5D1 mice as described (71). Following cell lysis
276 and MHC I immunoprecipitation, MAPs were analyzed by liquid chromatography MS/MS (Figure 6a).
277 To identify TE-coded MAPs, we generated a TE proteome by *in silico* translation of TE transcripts
278 expressed by mTECs or cTECs, and this TE proteome was concatenated with the canonical proteome.
279 MS analyses enabled the identification of a total of 1636 and 1714 MAPs in mTECs and cTECs,
280 respectively. From these, we identified 4 TE-derived MAPs in mTECs and 2 in cTECs, demonstrating
281 that TEs can be translated and presented by MHC I in the thymic cortex and medulla (Figure 6b and
282 Supplementary file 1 – Table 10). These MAPs were coded by the three major groups of TE: LINEs
283 (n=1), LTRs (n=1), and SINEs (n=4). Next, we evaluated whether the low number of TE MAPs
284 identified could result from mass spectrometry detection limits (72, 73). We measured the level and
285 frequency of TE expression in two subsets of cTECs (Figure 6c, left) or mTECs (Figure 6c, right) using
286 scRNA-seq data from *Baran-Gale et al.* (74). TE subfamilies generating MAPs in cTECs or mTECs are
287 highlighted in red in their respective plots. Strikingly, TECs highly and ubiquitously expressed the
288 MAP-generating TE subfamilies. These results suggest that the contribution of TEs to the MAP
289 repertoire of cTECs and mTECs might be significantly underestimated by the limits of detection of MS.
290 This is particularly true for mTECs because they express high levels of TEs (Figure 3d), but their TE

291 profile displays considerable intercellular heterogeneity (Figure 3e and Figure 3 – figure supplement 2).
292 Nonetheless, our data provide direct evidence that TEs can generate MAPs presented by cTECs and
293 mTECs, which can contribute to thymocyte education.

294

295 **Discussion**

296 TEs are germline-integrated parasitic DNA elements that comprise about half of mammalian genomes.
297 Over evolutionary timescales, TE sequences have been co-opted for host regulatory functions.
298 Mechanistically, TEs encode proteins and noncoding RNAs that regulate gene expression at multiple
299 levels (32, 75). Regulation of IFN signaling and triggering innate sensors are the best-characterized roles
300 of TEs in the mammalian immune system (36). TEs are immunogenic and can elicit adaptive immune
301 responses implicated in autoimmune diseases (34, 36, 76, 77). Pervasive TE expression in various
302 somatic organs means that co-evolution with their host must depend on establishing immune tolerance, a
303 concept supported by the highly diversified TE repertoire expressed in mTECs (34). This observation
304 provided the impetus to perform multi-omic studies of TE expression in the thymus. At the whole organ
305 level, we found that TE expression showed extensive age- and cell lineage-related variations and was
306 negatively correlated with cell proliferation and expression of KZFPs. The negative correlation between
307 TE expression and cell cycle scores in the thymus is coherent with recent data showing that
308 transcriptional activity of L1s is increased in senescent cells (78). A potential rationale for this could be
309 to prevent deleterious transposition events during DNA replication and cell division. On the other hand,
310 the contribution of KZFPs to TE regulation in the thymus is likely underestimated due to their typically
311 low expression (79) and scRNA-seq detection limit. Additionally, TEs interact with multiple TFs in all
312 thymic cell subsets. This is particularly true for the LINE and SINE subfamilies that occupy larger

313 genomic spaces. Notably, TEs appear to play particularly important roles in two cell types located in the
314 thymic medulla: mTECs and pDCs.

315

316 As mTECs are the APC population crucial to central tolerance induction, their high and diverse TE
317 expression is poised to impact the T cell repertoire's formation profoundly. The extent and complexity of
318 TF-TE interactions were higher in mTECs than in all other thymic cell subsets. These interactions
319 included *PAX1* and subunits of the NF-κB complex (e.g., *RELB*). *PAX1* is essential for the development
320 of TEC progenitors (50), and *RELB* is for the development and differentiation of mTECs (80). *RelB*-
321 deficient mice have reduced thymic cellularity, markedly fewer mTECs, lack *Aire* expression, and suffer
322 from autoimmunity (49, 81). Under the influence of *Aire*, *Fezf2*, and *Chd4*, mTECs collectively express
323 almost the entire exome (63, 64). However, the expression of all genes in each mTEC would cause
324 proteotoxic stress (64). Hence, promiscuous expression of tissue-restricted genes in mTECs adopts a
325 mosaic pattern: individual tissue-restricted genes are expressed in a small fraction of mTECs (17, 82).
326 The present work shows that mTECs also express an extensive repertoire of TEs in a mosaic pattern
327 (i.e., with considerable intercellular heterogeneity). *Aire*, *Fezf2*, and *Chd4* regulate non-redundant sets of
328 TEs and preferentially induce TE sequences associated with permissive histone marks. The
329 immunopeptidome of thymic stromal cells is responsible for thymocyte education and represents one of
330 the most fundamental “known unknowns” in immunology. Inferences on the immunopeptidome of
331 thymic stromal cells are based on transcriptomic data. However, i) TCRs interact with MAPs, not
332 transcripts, and ii) the MAP repertoire cannot be inferred from the transcriptome (65, 83, 84). Using
333 K5D1 mice presenting prominent thymic hyperplasia, we conducted MS searches of TE MAPs,
334 identifying 4 TE MAPs in mTECs and 2 in cTECs. These results demonstrate that cTECs and mTECs
335 present TE MAPs and suggest they present different TE MAPs. However, the correlation between

336 transcriptomic and immunopeptidomic data suggests that TECs can present many more TE MAPs. Their
337 profiling will require MS analyses of enormous numbers of TECs or the development of more sensitive
338 MS techniques. As TE MAPs have been detected in normal and neoplastic extrathymic cells (34, 85-87),
339 the presentation of TEs by mTECs is likely essential to central tolerance. In line with vibrant plaidoyers
340 for a collaborative Human Immunopeptidome Project (66, 88), our work suggests that
341 immunopeptidomic studies should not be limited to protein-coding genes (2% of the genome) but also
342 encompass non-coding sequences such as TEs.

343

344 The second population of cells exhibiting high TE expression, pDCs, are mainly seen as producers of
345 IFN α/β and potentially as APCs (21). Thymic and extrathymic pDCs are ontogenically and
346 functionally different. They develop independently from each other from different precursor cells (23,
347 24, 89). IFN α/β secretion is inducible in extrathymic pDCs but constitutive in thymic pDCs (21, 22). In
348 line with the location of pDCs in the thymic medulla, their constitutive IFN α/β secretion is
349 instrumental in the terminal differentiation of thymocytes and the generation of Tregs and innate CD8 T
350 cells (25-29). We report here that high TE expression is also a feature of thymic, but not extrathymic,
351 pDCs. Thus, the present study provides a rationale for the constitutive IFN α/β secretion by thymic
352 pDCs: they homogeneously express large numbers of TEs (in particular LINEs and SINEs), leading to
353 the formation of dsRNAs that trigger RIG-I and MDA5 signaling that causes the constitutive secretion
354 of IFN α/β . As such, our data suggest that recognition of TE-derived dsRNAs by innate immune
355 receptors promotes a pro-inflammatory environment favorable to the establishment of central tolerance
356 in the thymic medulla.

357

358 At first sight, the pleiotropic effects of TEs on thymic function may look surprising. It should be
359 reminded that the integration of genetic parasites such as TEs is a source of genetic conflicts with the
360 host. Notably, the emergence of adaptive immunity gave rise to higher-order conflicts between TEs and
361 their vertebrate hosts (36, 90). The crucial challenge for the immune system is developing immune
362 tolerance towards TEs to prevent autoimmune diseases that affect up to 10% of humans (91) without
363 allowing selfish retrotransposition events that hinder genome integrity. The resolution of these conflicts
364 has been proposed to be a determining factor in shaping the function of the immune system (90). Our
365 data suggest that the thymus is the central battlefield for conflict resolution between TEs and T cells in
366 vertebrates. Consistent with the implication of TEs in autoimmunity, more than 90% of putative causal
367 variants associated with autoimmune diseases are in allegedly noncoding regions of the genome (91). In
368 this context, our study illustrates the complexity of interactions between TEs and the vertebrate immune
369 system and should provide impetus to explore them further in health and disease. We see two limitations
370 to our study. First, as with all multi-omic systems immunology studies, our work provides a roadmap for
371 many future mechanistic studies that could not be realized at this stage. Second, our immunopeptidomic
372 analyses of TECs prove that TECs present TE MAPs but certainly underestimate the diversity of TE
373 MAPs presented by cTECs and mTECs.

374 **Methods**

375 **Experimental design**

376 This study aimed to understand better the impacts of TE expression on thymus development and
377 function. Thymic populations are complex and heterogeneous, so we opted for single-cell RNA-seq data
378 to draw a comprehensive profile of TE expression in the thymus. To better understand the impact of
379 AIRE, FEZF2, and CHD4 on TE expression in the mTEC(II) population, RNA-seq data from WT and
380 KO murine mTEC, as well as ChIP-seq for different histone marks in murine mTECs, were reanalyzed

381 to characterize the TE sequences regulated by these three proteins. Unless stated otherwise, studies were
382 done in human cells. For MS analyses, two replicates of 70 million cells from K5D1 mice (68) were
383 injected for both cTECs and mTECs. All experiments were in accordance with the Canadian Council on
384 Animal Care guidelines and approved by the *Comité de Déontologie de l'Expérimentation sur des*
385 *Animaux* of Université de Montréal. Primary human thymi were obtained from 4-month-old to 12-year-
386 old children undergoing cardiovascular surgeries at the CHU Sainte-Justine. This project was approved
387 by the CHU Sainte-Justine Research Ethics Board (protocol and biobank #2126).

388 **Transcriptomic data processing**

389 Preprocessing of the scRNA-seq data was performed with kallisto (92), which uses an expectation-
390 maximization algorithm to reassign multimapping reads based on the frequency of unique mappers at
391 each sequence and bustools workflow. For human thymic data from *Park et al.* (42) and splenic data
392 from *Madissoon et al.* (61), two different indexes were built for the pseudoalignment of reads with
393 kallisto (version 0.46.0): one containing Ensembl 88 (GRCh38.88) transcripts used for the annotation of
394 cell populations, and a second containing Ensembl 88 transcripts and human TE sequences (LINE, LTR,
395 SINE) from RepeatMasker (93) which was used for all subsequent analyses of TE expression. For
396 murine data from *Baran-Gale et al.* (74), cell-type annotations from the original publication were used,
397 and an index containing mm10 transcripts and murine TE sequences from RepeatMasker was used to
398 analyze TE expression. The cell barcodes were corrected, and the feature-barcode matrices were
399 generated with the correct count functions of bustools (version 0.39.3) (94). For murine bulk RNA-seq
400 data, an index composed of mm10 (GRCm38) transcripts and murine TE sequences from RepeatMasker
401 was used for quantification with kallisto.

402 **ChIP-seq data reanalysis**

403 ChIP-seq data for i) ETS1 in human NK cells, ii) AIRE in murine mTECs, and iii) several histone marks
404 of mTECs from WT mice were reanalyzed (see “**Availability of data and materials**” for the complete
405 list). ETS1 ChIP-seq reads were aligned to the reference *Homo sapiens* genome (GRCh38) using
406 bowtie2 (version 2.3.5) (95) with the --very-sensitive parameter. Multimapping reads were removed
407 using the samtools view function with the -q 10 parameter, and duplicate reads were removed using the
408 samtools markdup function with the -r parameter (96). Peak calling was performed with macs2 with the
409 -m 5 50 parameter (97). Peaks overlapping with the ENCODE blacklist regions (98) were removed with
410 bedtools intersect (99) with default parameters. Overlap of ETS1 peaks with TE sequences was
411 determined using bedtools intersect with default parameters. BigWig files were generated using the
412 bamCoverage function of deeptools2 (100), and genomic tracks were visualized in the USCS Genome
413 Browser (101). For the murine histone marks and AIRE data, reads were aligned to the reference *Mus*
414 *musculus* genome (mm10) using bowtie2 with the --very-sensitive parameter. Multimapping reads were
415 removed using the samtools view function with the -q 10 parameter, and duplicate reads were removed
416 using the samtools markdup function with the -r parameter. For histone marks, read coverage at the
417 sequence body and flanking regions (+/- 3000 base pairs) of TE loci induced by AIRE, FEZF2, and
418 CHD4 was visualized using ngs.plot.r (version 2.63) (102). For AIRE, peaks overlapping with the
419 ENCODE blacklist regions were removed with bedtools intersect, and overlap of peaks with TE
420 sequences was determined using bedtools intersect with default parameters.

421 **Cell population annotation**

422 Feature-barcode matrices were imported in R with SingleCellExperiment (version 1.12.0) (103). As a
423 quality control, cells with less than 2000 UMI detected, less than 500 genes detected, or more than 5%
424 reads assigned to mitochondrial genes were considered low quality and removed from the dataset with
425 scuttle (version 1.0.4) (104). Cells with more than 7000 genes detected were considered doublets and

426 removed. Normalization of cell size factors was performed with scran (version 1.18.7) (105), and log-
427 normalization of read counts was done with scuttle with default parameters. Variable regions of TCR
428 and IG genes, as well as ribosomal and cell cycle genes (based on *Park et al.* (42)), were removed, and
429 highly variable features were selected based on a mean-variance trend based on a Poisson distribution of
430 noise with scran. Adjustment of sequencing depths between batches and mutual nearest neighbors
431 (MNN) correction were computed with batchelor (version 1.6.3) (106). Cell clustering was performed
432 with scran using the Jaccard index for edge weighting and the Louvain method for community detection.
433 Lists of marker genes for human thymic cell populations and TEC subsets were taken from *Park et al.*
434 (42) and *Bautista et al.* (60), whereas marker genes of splenic populations were based on *Madissoon et*
435 *al.* (61).

436 **TE expression throughout thymic development**

437 The expression of TE subfamilies was obtained by summing the read counts of loci based on the
438 RepeatMasker annotations. For each TE subfamily in each cell population, expression levels amongst
439 developmental stages were normalized by dividing them with the maximal expression value. Next, the
440 Euclidean distance between each TE subfamily in each cell population (based on their normalized
441 expression across developmental stages) was computed, followed by unsupervised hierarchical
442 clustering. The tree was then manually cut into three clusters, and enrichment of LINE, LTR, and SINE
443 elements in these three clusters was determined using Fisher's exact tests. The cluster assigned to each
444 TE subfamily in each cell population was visualized in a circos plot using the circlize package (version
445 0.4.14) (107) in R, and the percentage of each cell population found in embryonic or postnatal samples.
446 Finally, we computed the frequency that each TE family was assigned to the three clusters, and the
447 maximal value was kept. As a control, a random distribution of the expression of 809 TE subfamilies in
448 18 cell populations was generated. A cluster (cluster 1, 2, or 3) was randomly attributed for each

449 combination of TE subfamily and cell type, and the maximal occurrence of a given cluster across cell
450 types was then computed for each TE subfamily. Finally, the LINE, LTR, and SINE elements
451 distributions were compared to the random distribution with Kolmogorov-Smirnov tests.

452 **Regulation of TE expression by cell proliferation and KZFPs**

453 Proliferation scores were generated for each dataset cell using the CellCycleScoring function of Seurat
454 (version 4.1.0). As per *Cowan et al.* (108), we combined previously published lists of G2M and S phase
455 marker genes (109) to compute the proliferation scores. For each thymic cell population, we calculated
456 the Spearman correlation between proliferation scores and the expression of TE subfamilies. The
457 Benjamini-Hochberg method was applied to correct for multiple comparisons. Correlations were
458 considered positive if the correlation coefficient was ≥ 0.2 and the adjusted p-value ≤ 0.05 , and negative if
459 the coefficient was ≤ -0.2 and the adjusted p-value ≤ 0.05 . We also computed the median of all correlation
460 coefficients for each cell population. We then assigned the class of each TE subfamily correlated with
461 cell proliferation and compared this distribution to the distribution of classes of all TE subfamilies in the
462 human genome. The percentage of overlap of the sets of TE subfamilies significantly correlated with
463 cell proliferation was determined. A list of 401 human KZFPs was downloaded from *Imbeault et al.*
464 (44). Spearman correlations between KZFP and TE expression were independently computed in each
465 cell population with the same methodology as the cell proliferation analysis, and Benjamini-Hochberg
466 correction for multiple comparisons was applied. The information on the enrichment of KZFPs within
467 TE subfamilies was downloaded from *Imbeault et al.* (44). Sharing of KZFP-TE pairs between cell
468 populations was represented using the circlize package.

469 **Estimation of TE sequences' age**

470 The sequence divergence (defined as the number of mismatches per thousand) was given by the milliDiv
471 value in RepeatMasker. The milliDiv values of each TE locus were divided by the substitution rate of its

472 host's genome (2.2×10^{-9} mutation/year for *Homo sapiens* and 4.5×10^{-9} mutation/year for *Mus musculus*
473 (110, 111)). Finally, the age of each TE subfamily was determined by averaging the age of all loci of the
474 subfamily.

475 **Interactions between TE subfamilies and transcription factors**

476 We downloaded a list of 1638 transcription factors (TF) manually curated by *Lambert et al.* (112). For
477 each cell population of the thymus, Spearman correlations were computed for each possible pair of TF
478 and TE subfamily, and the Benjamini-Hochberg method was applied to correct the p-values for multiple
479 comparisons. Correlations were considered significant if i) the correlation coefficient was ≥ 0.2 , ii) the
480 adjusted p-value was ≤ 0.05 , and iii) the TF was expressed by $\geq 10\%$ of the cells of the population. The
481 correlations were validated using a bootstrap procedure (1000 iterations) to ensure their reproducibility.
482 Briefly, we randomly selected n cells out of the n cells of a given population (while allowing cells to be
483 selected multiple times). The empirical p-value was determined by dividing the number of iterations
484 with a correlation coefficient < 0.2 by the total number of iterations (1000). In parallel, the curated
485 binding motifs of 945 TFs were downloaded from the JASPAR database. We then used the *Find*
486 *Individual Motif Occurrences* (FIMO) software (113) to identify the 100 000 genomic positions with the
487 most significant matches for the TF binding motif. These lists of binding motif positions were then
488 intersected with the positions of TE loci with the intersect function of BEDTools (version 2.29.2) (99),
489 and the percentage of TE loci of each subfamily harboring TF binding motifs was determined. Thus, in a
490 specific cell population of the thymus, a TF was considered as interacting with a TE subfamily if it
491 satisfied two criteria: i) its expression was correlated with the one of the TE family (spearman
492 coefficient ≥ 0.2 , adjusted p-value ≤ 0.05 and expression of TF in $\geq 10\%$ of cells), and ii) at least one
493 locus of the TE subfamily contained a binding motif of the TF. For each cell population, networks of
494 interactions between TF and TE subfamilies were generated with the network package (version 1.17.1)

495 (114) in R and represented with the ggnetwork package. For the sake of clarity, only the most significant
496 interactions were illustrated for each cell type (i.e., correlation coefficient ≥ 0.3 , TF binding sites in $\geq 1\%$
497 of the loci of the TE subfamily, and TF expression in $\geq 10\%$ of cells of the population). Sharing of TF-
498 TE interactions between cell populations was represented with a chord diagram using the circlize
499 package. For each TE subfamily, the number of interactions with TFs and the number of loci of the TE
500 subfamily in the human genome were determined. Wilcoxon-Mann-Whitney tests were used to compare
501 the number of interactions with TF of LTR, LINE, and SINE elements, whereas Kendall tau correlation
502 was calculated between the number of interactions with TF and the number of loci of TE subfamilies.

503 **Identification of TE promoter and enhancer candidates**

504 From the previously identified list of TF-TE interactions, we isolated the specific loci containing TF
505 binding sites from the subfamilies whose expression was positively correlated with the TF. To determine
506 if these TE loci could act as promoters or enhancers, we used histone ChIP-seq data from the ENCODE
507 consortium for H3K27ac, H3K4me1, and H3K4me3. BED files from the ENCODE consortium were
508 downloaded for eight immune cell populations: B cells, CD4 Single Positive T cells (CD4 SP), CD8
509 Single Positive T cells (CD8 SP), dendritic cells (DC), monocytes and macrophages (Mono/Macro), NK
510 cells, Th17, and Treg. TE loci colocalizing with peaks in histone ChIP-seq data were identified using the
511 intersect function of BEDTools (version 2.29.2). To be considered enhancer candidates, TE loci had to
512 colocalize with H3K27ac and H3K4me1 but not H3K4me3. To be considered as promoter candidates,
513 TE loci had to colocalize with H3K27ac and H3K4me3, but not H3K4me1, and be located at ≤ 1000
514 nucleotides from a transcription start site (TSS) annotated in the refTSS database (115).

515 **Diversity of TE expression**

516 The human thymic scRNA-seq dataset was subsampled to retain only postnatal cells, as it was shown by
517 *Bornstein et al.* (56) that thymic APCs are mainly found in postnatal samples. The diversity of TE

518 sequences expressed by thymic populations was assessed using Shannon entropy. Using the vegan
519 package (version 2.5-7) (116) in R, two distinct Shannon entropy metrics were computed for each cell
520 population. First, the Shannon entropy was computed based on the expression level (i.e., $\log(\text{read}$
521 $\text{count})$) of TE subfamilies for each cell individually. The median entropy was calculated for each cell
522 population. In parallel, the diversity of TE sequences expressed by an entire population was also
523 assessed. For this purpose, a binary code was generated to represent the expression status of TE
524 subfamilies in each cell (where 1 is expressed and 0 is not expressed). For each population separately,
525 the binary codes of individual cells were summed to obtain the frequency of expression of each TE
526 subfamily in the population, which was used to compute the Shannon entropy of TE sequences
527 expressed by the population. A linear model was generated with the lm function of the stats package in
528 R to summarize the data distribution. The deviation (Δy) from the observed population's TE diversity
529 and the one expected by the linear model was computed for each cell population.

530 **TE expression in thymic APC**

531 A differential expression analysis of TE subfamilies between the subsets of thymic APC was performed
532 with the FindAllMarkers function with default parameters of Seurat (117) with the MAST model.
533 Finally, the heterogeneity of TE expression inside thymic APC subsets was evaluated with the MetaCell
534 package (version 0.3.5) (118). The composition of the metacells was validated based on manual
535 annotation (see the “Single-cell RNA-seq preprocessing” section), and only metacells with >50% of
536 cells belonging to the same subset of thymic APCs were kept. Differential expression of TE subfamilies
537 between metacells was performed as described above, and the percentage of overlap between the sets of
538 TEs overexpressed by the different metacells was computed.

539 **Isolation of human thymic pDCs and immunostaining of dsRNAs**

540 Primary human thymi were obtained from 4-month-old to 12-year-old children undergoing
541 cardiovascular surgeries at the CHU Sainte-Justine. This project was approved by the CHU Sainte-
542 Justine Research Ethics Board (protocol and biobank #2126). Thymi from 4-month-old to 12-year-old
543 individuals were cryopreserved in liquid nitrogen in the following solution: 95% (PBS-5% Dextran 40
544 (Sigma-Aldrich)) – 5% DMSO (Fisher Scientific). Protocol for thymic pDCs isolation was based on
545 *Stoeckle et al.* (119). Briefly, thymic samples were cut in ~2mm pieces, followed by three rounds of
546 digestion (40 min, 180 RPM at 37°C) in RPMI 1640 (Gibco) supplemented with 2mg/mL of Collagenase
547 A (Roche) and 0.1mg/mL of DNase I (Sigma-Aldrich). APCs were then enriched using Percoll (Sigma-
548 Aldrich) density centrifugation (3500g, 35min at 4°C), followed by an FBS cushion density gradient
549 (5mL of RPMI 1640 containing enriched APCs layered on 5mL of heat-inactivated FBS (Invitrogen,
550 12483020), 1000RPM for 10min at 4°C) to remove cell debris. Finally, thymic pDCs were magnetically
551 enriched using the QuadroMACS Separator (Miltenyi). Cells were stained with a CD303 (BDCA-2)
552 MicroBead Kit (Miltenyi), and labeled cells were loaded on LS columns (Miltenyi) for magnetic-
553 activated cell sorting.

554 Purified thymic pDCs were pipetted on poly-L-lysine (Sigma-Aldrich, 1:10 in dH₂O) coated 15µ-Slide 8
555 well (ibid) and incubated for 2h at 37°C in RPMI 1640 supplemented with 10% BSA (Sigma-Aldrich).
556 Cells were fixed using 1% [w/v] paraformaldehyde (PFA, Sigma-Aldrich) in PBS 1X (Sigma-Aldrich)
557 for 30min at room temperature. Cells were permeabilized for 30min at room temperature with 0.1%
558 [v/v] Triton X-100 (Sigma-Aldrich) in PBS 1X, followed by blocking using 5% [w/v] BSA (Sigma-
559 Aldrich) in PBS 1X for 30min at room temperature. Immunostaining was performed in four steps to
560 avoid unspecific binding of the secondary antibodies: i) incubation overnight at 4°C with the mouse
561 monoclonal IgG2a J2 antibody anti-dsRNA (Jena Bioscience, cat. RNT-SCI-10010500, dilution 1:200),
562 ii) incubation with the donkey anti-mouse IgG (H+L) antibody coupled to Alexa Fluor 555 (Invitrogen,

563 cat. A-31570, dilution 1:500) for 30min at room temperature, iii) incubation with the mouse monoclonal
564 IgG1 clone 6H6 anti-CD123 (eBioscience, cat. 14-1239-82, 1:100) for one hour at room temperature,
565 and iv) incubation with the goat anti-mouse IgG1 polyclonal Alexa Fluor 488 antibody (Invitrogen, cat.
566 A-21121, 1:1000) for 30min at room temperature. Finally, cells were stained with DAPI (Invitrogen, cat.
567 D3571, 1:1000) for 5 minutes at room temperature. All antibodies and DAPI were diluted in a blocking
568 solution. Image acquisition was made with an LSM 700 laser scanning confocal microscope (Zeiss)
569 using a 40x oil objective (Zeiss, Plan-Neofluar N.A. 1.4) and the ZEN software. Using the whiteTopHat
570 function of the EBImage package and the sigmoNormalize function of the MorphoR package in R, the
571 background of the DAPI signal was removed. The nuclei were segmented on the resulting images as
572 circular shapes based on the DAPI signal. The mean intensity of CD123 and J2 staining was determined
573 for each cytoplasm, defined as 19nm rings around nuclei. Based on the distribution of the CD123 signal
574 across cells, a threshold between CD123⁻ and CD123⁺ cells was set up for each replicate independently.
575 J2 signal intensity was compared between CD123⁻ and CD123⁺ cells using the Wilcoxon Rank Sum test
576 in R.

577 **Gene set enrichment analysis**

578 Gene set enrichment analyses were performed to determine which biological processes are enriched in
579 mTEC(II) and pDCs. Differential gene expression analyses were performed between each possible pair
580 of thymic APCs subsets using MAST with the FindMarkers function of Seurat. The gene set enrichment
581 analysis was performed using the iDEA package (version 1.0.1) (120) in R. As per *Ma et al.* (120), the
582 fold change and standard error of gene expression were used as input for iDEA, in addition to predefined
583 lists of gene sets compiled in the iDEA package. Gene sets associated with antigen presentation,
584 interferon signaling, and immune response were manually annotated. iDEA was launched with default
585 parameters, except for the 500 iterations of the Markov chain Monte Carlo algorithm, and p-values were

586 corrected with the Louis method. We also visualized the expression of *AIRE*, *FEZF2*, and *CHD4* in the
587 TEC lineage to validate their expression in mTEC(II).

588 **TE loci regulated by AIRE, FEZF2, and CHD4**

589 A differential expression analysis of TE subfamilies between WT and *Aire*-, *Fezf2*-, or *Chd4*-KO mice
590 was performed with the voom method of the limma package (version 3.46.0) (121, 122). Stringent
591 criteria (i.e., an expression below 2 transcripts per million (TPM) in all samples) were applied to remove
592 lowly expressed TEs. TE subfamilies with i) a fold change ≥ 2 and an adjusted p-value ≤ 0.05 or ii) a fold
593 change ≤ -2 and an adjusted p-value ≤ 0.05 were considered as induced and repressed, respectively. The
594 percentage of overlap between the sets of TE loci induced or repressed by AIRE, FEZF2, and CHD4
595 was computed. The class and subfamily were assigned to each regulated TE locus, and the distributions
596 of classes and subfamilies across all TE sequences of the murine genome were used as controls.
597 Significant enrichment of classes or subfamilies was determined with Chi-squared tests, and a
598 Bonferroni correction for multiple comparisons was performed to enrich subfamilies in induced or
599 repressed TEs. The distance between TE loci induced or repressed by AIRE, FEZF2, or CHD4 was
600 defined as the minimal distance between the middle position of TE loci on the same chromosome. As a
601 control, distributions of randomly selected TE loci whose expression is independent of AIRE, FEZF2,
602 and CHD4 and equal size to the sets of regulated TEs were generated (for example, if 433 TE loci are
603 induced by CHD4, 433 independent TE loci were randomly selected). Wilcoxon rank-sum tests were
604 used to compare random and regulated distributions. Genomic positions of exons, introns 3' and 5'
605 untranslated transcribed region (UTR) were downloaded from the UCSC Table Browser. The genomic
606 localization of regulated TEs was determined using the intersect mode of the BEDTools suite version
607 2.29.2. TE loci not located in exons, introns, 3'UTR, or 5'UTR were considered intergenic. The
608 percentage of regulated TE loci in each type of genomic region was determined and compared to the

609 genomic localization of all TE loci in the murine genome with chi-squared tests. Finally, we estimated
610 the frequency of intron retention events for introns containing TE loci regulated by AIRE, FEZF2, or
611 CHD4 with S-IRFindeR (123). Sequencing reads were aligned to the reference *Mus musculus* genome
612 (mm10) using STAR version 2.7.1a (124) with default parameters. Each intron's Stable Intron Retention
613 ratio (SIRratio) was computed with the computeSIRratio function of S-IRFindeR. Introns containing TE
614 loci induced by AIRE, FEZF2, or CHD4 were filtered using BEDTools intersect. Random distributions
615 of equivalent sizes of introns containing TE sequences independent of AIRE, FEZF2, and CHD4 were
616 generated as control. A SIRratio of 0.1 was used as a threshold of significant intron retention events.

617 **Enzymatic digestion and isolation of murine TECs**

618 Thymic stromal cell enrichment was performed as previously described (71, 125). Briefly, thymi from
619 16- to 22-week-old K5D1 mice were mechanically disrupted and enzymatically digested with papain
620 (Worthington Biochemical Corporation), DNase I (Sigma-Aldrich), and collagenase IV (Sigma-Aldrich)
621 at 37°C. Next, the single-cell suspension obtained after enzymatic digestion was maintained at 4°C in
622 FACS buffer (PBS, 0.5% [w/v] BSA, 2mM EDTA) and enriched in thymic epithelial cells using anti-
623 EpCAM (CD326) or anti-CD45 microbeads (mouse, Miltenyi) and LS columns (Miltenyi). Then, the
624 enriched epithelial cell suspension was stained for flow cytometry cell sorting with the following
625 antibodies and dyes: anti-EpCAM-APC-Cy7 clone G8.8 (BioLegend, cat. 118218), anti-CD45-APC
626 clone 30-F11 (BD Biosciences, cat. 559864), anti-UEA1-biotinylated (Vector Laboratories, cat. B-
627 1065), anti-I-A/I-E-Alexa Fluor 700 clone M5/114.15.2 (BioLegend, cat. 107622), anti-Ly51-FITC
628 clone 6C3 (BioLegend, cat. 553160), anti-streptavidin-PE-Cy7 (BD Biosciences, cat. 557598), and 7-
629 AAD (BD Biosciences, cat. 559925). Cell sorting was performed using a BD FACSaria (BD
630 Biosciences), and data were analyzed using the FACSDiva. TECs were defined as EpCAM⁺CD45⁻,
631 while the cTEC and mTEC subsets were defined as UEA1⁻Ly51⁺ and UEA1⁺Ly51⁻ TEC, respectively.

632 **RNA-Sequencing**

633 Total RNA from 80 000 mTECs or cTECs was isolated using TRIzol and purified with an RNeasy
634 micro kit (Qiagen). Total RNA was quantified using Qubit (Thermo Scientific), and RNA quality was
635 assessed with the Agilent 2100 Bioanalyzer (Agilent Technologies). Transcriptome libraries were
636 generated using a KAPA RNA HyperPrep kit (Roche) using a poly(A) selection (Thermo Scientific).
637 Sequencing was performed on the Illumina NextSeq 500, obtaining ~200 million paired-end reads per
638 sample.

639 **Preparation of CNBR-activated Sepharose beads for MHC I immunoprecipitation**

640 CNBR-activated Sepharose 4B beads (Sigma-Aldrich, cat. 17-0430-01) were incubated with 1 mM HCl
641 at a ratio of 40 mg of beads per 13.5 ml of 1 mM HCl for 30 minutes with tumbling at room
642 temperature. Beads were spun at 215g for 1 minute at 4°C, and supernatants were discarded. 40 mg of
643 beads were resuspended with 4 ml of coupling buffer (0.1M NaHCO₃/0.5M NaCl pH 8.3), spun at 215g
644 for 1 minute at 4°C, and the supernatants were discarded. Mouse antibodies Pan-H2 (clone M1/42), H2-
645 K^b (clone Y-3), and H2-D^b (clone 28-14-8S) were coupled to beads at a ratio of 1 mg of antibody to 40
646 mg of beads in coupling buffer for 120 minutes with tumbling at room temperature. Beads were spun at
647 215g for 1 minute at 4°C, and supernatants were discarded. 40 mg of beads were resuspended with 1 ml
648 of blocking buffer (0.2M glycine), incubated for 30 minutes with tumbling at room temperature, and the
649 supernatants were discarded. Beads were washed by centrifugation twice with PBS pH 7.2, resuspended
650 at a concentration of 1 mg of antibody per ml of PBS pH 7.2, and stored at 4°C.

651 **Immuno-isolation of MAPs**

652 Frozen pellets of mTECs (90 mice, 191 million cells total) and cTECs (121 mice, 164 million cells total)
653 were thawed, pooled, and resuspended with PBS pH 7.2 up to 4 ml and then solubilized by adding 4 mL
654 of detergent buffer containing PBS pH 7.2, 1% (w/v) CHAPS (Sigma, cat. C9426-5G) supplemented

655 with Protease inhibitor cocktail (Sigma, cat. P8340-5mL). Solubilized cells were incubated for 60
656 minutes with tumbling at 4°C and then spun at 16,600g for 20 minutes at 4°C. Supernatants were
657 transferred into new tubes containing 1.5 mg of Pan-H2, 0.5 mg of H2-K^b, and 0.5 mg of H2-D^b
658 antibodies covalently-cross-linked CNBR-Sepharose beads per sample and incubated with tumbling for
659 180 minutes at 4°C. Samples were transferred into BioRad Poly prep chromatography columns and
660 eluted by gravity. Beads were first washed with 11.5 mL PBS, then with 11.5 mL of 0.1X PBS, and
661 finally with 11.5 mL of water. MHC I complexes were eluted from the beads by acidic treatment using
662 1% trifluoroacetic acid (TFA). Acidic filtrates containing peptides were separated from MHC I subunits
663 (HLA molecules and β-2 microglobulin) using home-made stage tips packed with two 1 mm diameter
664 octadecyl (C-18) solid phase extraction disks (EMPORE). Stage tips were pre-washed with methanol,
665 then with 80% acetonitrile (ACN) in 0.1% TFA, and finally with 1% TFA. Samples were loaded onto
666 the stage tips and washed with 1% TFA and 0.1% TFA. Peptides were eluted with 30% ACN in 0.1%
667 TFA, dried using vacuum centrifugation, and then stored at -20 °C until MS analysis.

668 **MS analyses**

669 Peptides were loaded and separated on a home-made reversed-phase column (150-μm i.d. by 200 mm)
670 with a 106-min gradient from 10 to 38% B (A: formic acid 0.1%, B: 80% CAN 0.1% formic acid) and a
671 600-nL/min flow rate on an Easy nLC-1200 connected to an Orbitrap Exploris 480 (Thermo Fisher
672 Scientific). Each full MS spectrum acquired at a resolution of 240,000 was followed by tandem-MS
673 (MS-MS) spectra acquisition on the most abundant multiply charged precursor ions for a maximum of
674 3s. Tandem-MS experiments were performed using higher energy collision-induced dissociation (HCD)
675 at a collision energy of 34%. The generation of the personalized proteome containing TE sequences, as
676 well as the identification of TE-derived MAPs, was performed as per *Larouche et al.* (34) with the
677 following modifications: the mm10 murine reference genome was downloaded from the UCSC Genome

678 Browser, the annotations for murine genes and TE sequences were downloaded from the UCSC Table
679 Browser, and the Uniprot mouse database (16 977 entries) was used for the canonical proteome. MAPs
680 were identified using PEAKS X Pro (Bioinformatics Solutions, Waterloo, ON). The level and frequency
681 of expression of TE subfamilies generating MAPs or not were determined in thymic epithelial cells were
682 determined by averaging the expression values across cells of a TEC subset and dividing the number of
683 cells with a positive (i.e.,> 0) expression of the TEs by the total number of cells of the TEC subset,
684 respectively.

685 **Availability of data and materials:**

686 scRNA-seq data of human thymi and spleen were downloaded from ArrayExpress (accession number E-
687 MTAB-8581) and the NCBI BIOPROJECT (accession code PRJEB31843), respectively. scRNA-seq
688 data of murine thymi were downloaded from ArrayExpress (accession number E-MTAB-8560). RNA-
689 seq data from WT, Aire-KO, Fezf2-KO, and Chd4-KO murine mTECs were downloaded from the Gene
690 Expression Omnibus (GEO) under the accession code GSE144880. ChIP-seq data of ETS1 in human
691 NK cells and AIRE in murine mTECs were downloaded from GEO (accession codes GSE124104 and
692 GSE92654, respectively). ChIP-seq data for different histone marks in murine mTECs were also
693 downloaded from GEO: H3K4me3 for mTECs (GSE53111); H3K4me1 and H3K27ac from MHCII^{hi}
694 mTECs (GSE92597); H3K4me2 in mTEC-II (GSE103969); and H3K4ac and H3K9ac in mTECs
695 (GSE114713). Transcriptomic and immunopeptidomic data of K5D1 mice mTECs and cTECs generated
696 in this study are available on the Gene Expression Omnibus (GEO) under the accession GSE232011 and
697 on the Proteomics Identification Database (PRIDE) under the accession PXD042241, respectively.

698 **Author contributions:**

699 Conceptualization: JDL, CML, AT, KV, CP

700 Methodology: JDL, CML, AT, KV

701 Investigation: JDL, LH, CC, SB, JH, EB, JL, CD, PG, JPL
702 Visualization: JDL, CML, AT
703 Funding acquisition: JDL, CP
704 Project administration: JDL, KV, CP
705 Supervision: SL, PT, CP
706 Writing – original draft: JDL, KV, CP
707 Writing – review & editing: JDL, CML, AT, KV, LH, JH, SB, CC, EB, JL, CD, PG, ERR, BHN, SL,
708 PT, CP

709 **Acknowledgments:**

710 The authors thank Christian Charbonneau and Raphaëlle Lambert from IRIC's bio-imaging and
711 genomics platforms, respectively. We also thank Allan Sauvat for the help with the microscopy
712 quantification. We thank Mathilde Soulez, Bernhard Lehnertz, Biljana Culjkovic, Brian Wilhelm, and
713 Michaël Imbeault for insightful discussions. We are indebted to Kathie Béland and Elie Haddad from
714 the CHU Sainte-Justine Research Center for providing the primary thymic samples.

715

716 **References**

- 717 1. Boehm T. Evolution of vertebrate immunity. *Curr Biol*. 2012;22(17):R722-32.
- 718 2. Boehm T, Swann JB. Origin and evolution of adaptive immunity. *Annu Rev Anim Biosci*.
719 2014;2:259-83.
- 720 3. Suo C, Dann E, Goh I, Jardine L, Kleshchevnikov V, Park JE, et al. Mapping the developing
721 human immune system across organs. *Science*. 2022;376(6597):eab00510.
- 722 4. Terra R, Louis I, Le Blanc R, Ouellet S, Zuniga-Pflucker JC, Perreault C. T-cell generation by
723 lymph node resident progenitor cells. *Blood*. 2005;106(1):193-200.
- 724 5. Blais ME, Brochu S, Giroux M, Belanger MP, Dulude G, Sekaly RP, et al. Why T cells of
725 thymic versus extrathymic origin are functionally different. *J Immunol*. 2008;180(4):2299-312.
- 726 6. Zuniga-Pflucker JC, Longo DL, Kruisbeek AM. Positive selection of CD4-CD8+ T cells in the
727 thymus of normal mice. *Nature*. 1989;338(6210):76-8.

728 7. Breed ER, Lee ST, Hogquist KA. Directing T cell fate: How thymic antigen presenting cells
729 coordinate thymocyte selection. *Semin Cell Dev Biol.* 2018;84:2-10.

730 8. Dervovic D, Zuniga-Pflucker JC. Positive selection of T cells, an in vitro view. *Semin Immunol.*
731 2010;22(5):276-86.

732 9. Lebel ME, Coutelier M, Galipeau M, Kleinman CL, Moon JJ, Melichar HJ. Differential
733 expression of tissue-restricted antigens among mTEC is associated with distinct autoreactive T cell fates.
734 *Nat Commun.* 2020;11(1):3734.

735 10. Srinivasan J, Lancaster JN, Singarapu N, Hale LP, Ehrlich LIR, Richie ER. Age-Related
736 Changes in Thymic Central Tolerance. *Front Immunol.* 2021;12:676236.

737 11. Cheng M, Anderson MS. Thymic tolerance as a key brake on autoimmunity. *Nat Immunol.*
738 2018;19(7):659-64.

739 12. Perera J, Zheng Z, Li S, Gudjonson H, Kalinina O, Benichou JJC, et al. Self-Antigen-Driven
740 Thymic B Cell Class Switching Promotes T Cell Central Tolerance. *Cell Rep.* 2016;17(2):387-98.

741 13. Nitta T, Ohigashi I, Nakagawa Y, Takahama Y. Cytokine crosstalk for thymic medulla
742 formation. *Curr Opin Immunol.* 2011;23(2):190-7.

743 14. Malhotra D, Linehan JL, Dileepan T, Lee YJ, Purtha WE, Lu JV, et al. Tolerance is established
744 in polyclonal CD4(+) T cells by distinct mechanisms, according to self-peptide expression patterns. *Nat*
745 *Immunol.* 2016;17(2):187-95.

746 15. Lkhagvasuren E, Sakata M, Ohigashi I, Takahama Y. Lymphotoxin beta receptor regulates the
747 development of CCL21-expressing subset of postnatal medullary thymic epithelial cells. *J Immunol.*
748 2013;190(10):5110-7.

749 16. Laan M, Salumets A, Klein A, Reintamm K, Bichele R, Peterson H, et al. Post-Aire Medullary
750 Thymic Epithelial Cells and Hassall's Corporcles as Inducers of Tonic Pro-Inflammatory
751 Microenvironment. *Front Immunol.* 2021;12:635569.

752 17. Michelson DA, Hase K, Kaisho T, Benoist C, Mathis D. Thymic epithelial cells co-opt lineage-
753 defining transcription factors to eliminate autoreactive T cells. *Cell.* 2022.

754 18. Ramsey C, Winqvist O, Puhakka L, Halonen M, Moro A, Kampe O, et al. Aire deficient mice
755 develop multiple features of APECED phenotype and show altered immune response. *Hum Mol Genet.*
756 2002;11(4):397-409.

757 19. Takaba H, Morishita Y, Tomofuji Y, Danks L, Nitta T, Komatsu N, et al. Fezf2 Orchestrates a
758 Thymic Program of Self-Antigen Expression for Immune Tolerance. *Cell.* 2015;163(4):975-87.

759 20. Tomofuji Y, Takaba H, Suzuki HI, Benlaribi R, Martinez CDP, Abe Y, et al. Chd4 choreographs
760 self-antigen expression for central immune tolerance. *Nat Immunol.* 2020;21(8):892-901.

761 21. Ginhoux F, Guilliams M, Merad M. Expanding dendritic cell nomenclature in the single-cell era.
762 *Nat Rev Immunol.* 2022;22(2):67-8.

763 22. Colantonio AD, Epeldegui M, Jesiak M, Jachimowski L, Blom B, Uittenbogaart CH. IFN-alpha
764 is constitutively expressed in the human thymus, but not in peripheral lymphoid organs. *PLoS One.*
765 2011;6(8):e24252.

766 23. Lavaert M, Liang KL, Vandamme N, Park JE, Roels J, Kowalczyk MS, et al. Integrated scRNA-
767 Seq Identifies Human Postnatal Thymus Seeding Progenitors and Regulatory Dynamics of
768 Differentiating Immature Thymocytes. *Immunity.* 2020;52(6):1088-104 e6.

769 24. Le J, Park JE, Ha VL, Luong A, Branciamore S, Rodin AS, et al. Single-Cell RNA-Seq Mapping
770 of Human Thymopoiesis Reveals Lineage Specification Trajectories and a Commitment Spectrum in T
771 Cell Development. *Immunity.* 2020;52(6):1105-18 e9.

772 25. Xing Y, Wang X, Jameson SC, Hogquist KA. Late stages of T cell maturation in the thymus
773 involve NF-kappaB and tonic type I interferon signaling. *Nat Immunol.* 2016;17(5):565-73.

774 26. Hanabuchi S, Ito T, Park WR, Watanabe N, Shaw JL, Roman E, et al. Thymic stromal
775 lymphopoietin-activated plasmacytoid dendritic cells induce the generation of FOXP3+ regulatory T
776 cells in human thymus. *J Immunol.* 2010;184(6):2999-3007.

777 27. Martin-Gayo E, Sierra-Filardi E, Corbi AL, Toribio ML. Plasmacytoid dendritic cells resident in
778 human thymus drive natural Treg cell development. *Blood.* 2010;115(26):5366-75.

779 28. Martinet V, Tonon S, Torres D, Azouz A, Nguyen M, Kohler A, et al. Type I interferons regulate
780 eomesodermin expression and the development of unconventional memory CD8(+) T cells. *Nat
781 Commun.* 2015;6:7089.

782 29. Epeldegui M, Blom B, Uittenbogaart CH. BST2/Tetherin is constitutively expressed on human
783 thymocytes with the phenotype and function of Treg cells. *Eur J Immunol.* 2015;45(3):728-37.

784 30. Treangen TJ, Salzberg SL. Repetitive DNA and next-generation sequencing: computational
785 challenges and solutions. *Nat Rev Genet.* 2011;13(1):36-46.

786 31. Deniz O, Frost JM, Branco MR. Regulation of transposable elements by DNA modifications.
787 *Nat Rev Genet.* 2019;20(7):417-31.

788 32. Bourque G, Burns KH, Gehring M, Gorbunova V, Seluanov A, Hammell M, et al. Ten things
789 you should know about transposable elements. *Genome Biol.* 2018;19(1):199.

790 33. Argueso JL, Westmoreland J, Mieczkowski PA, Grawel M, Petes TD, Resnick MA. Double-
791 strand breaks associated with repetitive DNA can reshape the genome. *Proc Natl Acad Sci U S A.*
792 2008;105(33):11845-50.

793 34. Larouche JD, Trofimov A, Hesnard L, Ehix G, Zhao Q, Vincent K, et al. Widespread and tissue-
794 specific expression of endogenous retroelements in human somatic tissues. *Genome Med.*
795 2020;12(1):40.

796 35. Carter JA, Stromich L, Peacey M, Chapin SR, Velten L, Steinmetz LM, et al. Transcriptomic
797 diversity in human medullary thymic epithelial cells. *Nat Commun.* 2022;13(1):4296.

798 36. Kassiotis G. The Immunological Conundrum of Endogenous Retroelements. *Annu Rev
799 Immunol.* 2023;41:99-125.

800 37. Chuong EB, Elde NC, Feschotte C. Regulatory evolution of innate immunity through co-option
801 of endogenous retroviruses. *Science.* 2016;351(6277):1083-7.

802 38. Bogdan L, Barreiro L, Bourque G. Transposable elements have contributed human regulatory
803 regions that are activated upon bacterial infection. *Philos Trans R Soc Lond B Biol Sci.*
804 2020;375(1795):20190332.

805 39. Adoue V, Binet B, Malbec A, Fourquet J, Romagnoli P, van Meerwijk JPM, et al. The Histone
806 Methyltransferase SETDB1 Controls T Helper Cell Lineage Integrity by Repressing Endogenous
807 Retroviruses. *Immunity.* 2019;50(3):629-44 e8.

808 40. Lefkopoulos S, Polyzou A, Derecka M, Bergo V, Clapes T, Cauchy P, et al. Repetitive Elements
809 Trigger RIG-I-like Receptor Signaling that Regulates the Emergence of Hematopoietic Stem and
810 Progenitor Cells. *Immunity.* 2020;53(5):934-51 e9.

811 41. Lima-Junior DS, Krishnamurthy SR, Bouladoux N, Collins N, Han SJ, Chen EY, et al.
812 Endogenous retroviruses promote homeostatic and inflammatory responses to the microbiota. *Cell.*
813 2021.

814 42. Park JE, Botting RA, Dominguez Conde C, Popescu DM, Lavaert M, Kunz DJ, et al. A cell atlas
815 of human thymic development defines T cell repertoire formation. *Science.* 2020;367(6480).

816 43. Brocks D, Chomsky E, Mukamel Z, Lifshitz A, Tanay A. Single cell analysis reveals dynamics
817 of transposable element transcription following epigenetic de-repression. *bioRxiv.* 2018:462853.

818 44. Imbeault M, Helleboid PY, Trono D. KRAB zinc-finger proteins contribute to the evolution of
819 gene regulatory networks. *Nature.* 2017;543(7646):550-4.

820 45. Kunarso G, Chia NY, Jeyakani J, Hwang C, Lu X, Chan YS, et al. Transposable elements have
821 rewired the core regulatory network of human embryonic stem cells. *Nat Genet.* 2010;42(7):631-4.

822 46. Sundaram V, Cheng Y, Ma Z, Li D, Xing X, Edge P, et al. Widespread contribution of
823 transposable elements to the innovation of gene regulatory networks. *Genome Res.* 2014;24(12):1963-
824 76.

825 47. Hosokawa H, Rothenberg EV. How transcription factors drive choice of the T cell fate. *Nat Rev
826 Immunol.* 2021;21(3):162-76.

827 48. Baik S, Sekai M, Hamazaki Y, Jenkinson WE, Anderson G. Relb acts downstream of medullary
828 thymic epithelial stem cells and is essential for the emergence of RANK(+) medullary epithelial
829 progenitors. *Eur J Immunol.* 2016;46(4):857-62.

830 49. Akiyama T, Shimo Y, Yanai H, Qin J, Ohshima D, Maruyama Y, et al. The tumor necrosis factor
831 family receptors RANK and CD40 cooperatively establish the thymic medullary microenvironment and
832 self-tolerance. *Immunity.* 2008;29(3):423-37.

833 50. Yamazaki Y, Urrutia R, Franco LM, Giliani S, Zhang K, Alazami AM, et al. PAX1 is essential
834 for development and function of the human thymus. *Sci Immunol.* 2020;5(44).

835 51. Meixner A, Karreth F, Kenner L, Wagner EF. JunD regulates lymphocyte proliferation and T
836 helper cell cytokine expression. *EMBO J.* 2004;23(6):1325-35.

837 52. Cisse B, Caton ML, Lehner M, Maeda T, Scheu S, Locksley R, et al. Transcription factor E2-2 is
838 an essential and specific regulator of plasmacytoid dendritic cell development. *Cell.* 2008;135(1):37-48.

839 53. Choudhary MN, Friedman RZ, Wang JT, Jang HS, Zhuo X, Wang T. Co-opted transposons help
840 perpetuate conserved higher-order chromosomal structures. *Genome Biol.* 2020;21(1):16.

841 54. Consortium EP. An integrated encyclopedia of DNA elements in the human genome. *Nature.*
842 2012;489(7414):57-74.

843 55. Luo Y, Hitz BC, Gabdank I, Hilton JA, Kagda MS, Lam B, et al. New developments on the
844 Encyclopedia of DNA Elements (ENCODE) data portal. *Nucleic Acids Res.* 2020;48(D1):D882-D9.

845 56. Taveirne S, Wahlen S, Van Loocke W, Kiekens L, Persyn E, Van Ammel E, et al. The
846 transcription factor ETS1 is an important regulator of human NK cell development and terminal
847 differentiation. *Blood.* 2020;136(3):288-98.

848 57. Kim N, Kim M, Yun S, Doh J, Greenberg PD, Kim TD, et al. MicroRNA-150 regulates the
849 cytotoxicity of natural killers by targeting perforin-1. *J Allergy Clin Immunol.* 2014;134(1):195-203.

850 58. Gunturi A, Berg RE, Forman J. The role of CD94/NKG2 in innate and adaptive immunity.
851 *Immunol Res.* 2004;30(1):29-34.

852 59. Bornstein C, Nevo S, Giladi A, Kadouri N, Pouzolles M, Gerbe F, et al. Single-cell mapping of
853 the thymic stroma identifies IL-25-producing tuft epithelial cells. *Nature.* 2018;559(7715):622-6.

854 60. Bautista JL, Cramer NT, Miller CN, Chavez J, Berrios DI, Byrnes LE, et al. Single-cell
855 transcriptional profiling of human thymic stroma uncovers novel cellular heterogeneity in the thymic
856 medulla. *Nat Commun.* 2021;12(1):1096.

857 61. Madissoon E, Wilbrey-Clark A, Miragaia RJ, Saeb-Parsy K, Mahbubani KT, Georgakopoulos N,
858 et al. scRNA-seq assessment of the human lung, spleen, and esophagus tissue stability after cold
859 preservation. *Genome Biol.* 2019;21(1):1.

860 62. Sadeq S, Al-Hashimi S, Cusack CM, Werner A. Endogenous Double-Stranded RNA. Noncoding
861 RNA. 2021;7(1).

862 63. Sansom SN, Shikama-Dorn N, Zhanybekova S, Nusspaumer G, Macaulay IC, Deadman ME, et
863 al. Population and single-cell genomics reveal the Aire dependency, relief from Polycomb silencing, and
864 distribution of self-antigen expression in thymic epithelia. *Genome Res.* 2014;24(12):1918-31.

865 64. St-Pierre C, Morgand E, Benhammadi M, Rouette A, Hardy MP, Gaboury L, et al.
866 Immunoproteasomes Control the Homeostasis of Medullary Thymic Epithelial Cells by Alleviating
867 Proteotoxic Stress. *Cell Rep.* 2017;21(9):2558-70.

868 65. Shapiro IE, Bassani-Sternberg M. The impact of immunopeptidomics: From basic research to
869 clinical implementation. *Semin Immunol.* 2023;66:101727.

870 66. Vizcaino JA, Kubiniok P, Kovalchik KA, Ma Q, Duquette JD, Mongrain I, et al. The Human
871 Immunopeptidome Project: A Roadmap to Predict and Treat Immune Diseases. *Mol Cell Proteomics.*
872 2020;19(1):31-49.

873 67. Kubiniok P, Marcu A, Bichmann L, Kuchenbecker L, Schuster H, Hamelin DJ, et al.
874 Understanding the constitutive presentation of MHC class I immunopeptidomes in primary tissues.
875 *iScience.* 2022;25(2):103768.

876 68. Robles AI, Larcher F, Whalin RB, Murillas R, Richie E, Gimenez-Conti IB, et al. Expression of
877 cyclin D1 in epithelial tissues of transgenic mice results in epidermal hyperproliferation and severe
878 thymic hyperplasia. *Proc Natl Acad Sci U S A.* 1996;93(15):7634-8.

879 69. Klug DB, Crouch E, Carter C, Coghlan L, Conti CJ, Richie ER. Transgenic expression of cyclin
880 D1 in thymic epithelial precursors promotes epithelial and T cell development. *J Immunol.*
881 2000;164(4):1881-8.

882 70. Ohigashi I, Tanaka Y, Kondo K, Fujimori S, Kondo H, Palin AC, et al. Trans-omics Impact of
883 Thymoproteasome in Cortical Thymic Epithelial Cells. *Cell Rep.* 2019;29(9):2901-16 e6.

884 71. Dumont-Lagace M, Daouda T, Depoers L, Zumer J, Benslimane Y, Brochu S, et al. Qualitative
885 Changes in Cortical Thymic Epithelial Cells Drive Postpartum Thymic Regeneration. *Front Immunol.*
886 2019;10:3118.

887 72. Ghosh M, Gauger M, Marcu A, Nelde A, Denk M, Schuster H, et al. Guidance Document:
888 Validation of a High-Performance Liquid Chromatography-Tandem Mass Spectrometry
889 Immunopeptidomics Assay for the Identification of HLA Class I Ligands Suitable for Pharmaceutical
890 Therapies. *Mol Cell Proteomics.* 2020;19(3):432-43.

891 73. Nanaware PP, Jurewicz MM, Clement CC, Lu L, Santambrogio L, Stern LJ. Distinguishing
892 Signal From Noise in Immunopeptidome Studies of Limiting-Abundance Biological Samples: Peptides
893 Presented by I-A(b) in C57BL/6 Mouse Thymus. *Front Immunol.* 2021;12:658601.

894 74. Baran-Gale J, Morgan MD, Maio S, Dhalla F, Calvo-Asensio I, Deadman ME, et al. Ageing
895 compromises mouse thymus function and remodels epithelial cell differentiation. *Elife.* 2020;9.

896 75. Frank JA, Feschotte C. Co-option of endogenous viral sequences for host cell function. *Curr
897 Opin Virol.* 2017;25:81-9.

898 76. Groger V, Cynis H. Human Endogenous Retroviruses and Their Putative Role in the
899 Development of Autoimmune Disorders Such as Multiple Sclerosis. *Front Microbiol.* 2018;9:265.

900 77. Volkman HE, Stetson DB. The enemy within: endogenous retroelements and autoimmune
901 disease. *Nat Immunol.* 2014;15(5):415-22.

902 78. De Cecco M, Ito T, Petrashen AP, Elias AE, Skvir NJ, Criscione SW, et al. L1 drives IFN in
903 senescent cells and promotes age-associated inflammation. *Nature.* 2019;566(7742):73-8.

904 79. Huntley S, Baggott DM, Hamilton AT, Tran-Gyamfi M, Yang S, Kim J, et al. A comprehensive
905 catalog of human KRAB-associated zinc finger genes: insights into the evolutionary history of a large
906 family of transcriptional repressors. *Genome Res.* 2006;16(5):669-77.

907 80. Mouri Y, Nishijima H, Kawano H, Hirota F, Sakaguchi N, Morimoto J, et al. NF-kappaB-
908 inducing kinase in thymic stroma establishes central tolerance by orchestrating cross-talk with not only
909 thymocytes but also dendritic cells. *J Immunol.* 2014;193(9):4356-67.

910 81. O'Sullivan BJ, Yekollu S, Ruscher R, Mehdi AM, Maradana MR, Chidgey AP, et al.
911 Autoimmune-Mediated Thymic Atrophy Is Accelerated but Reversible in RelB-Deficient Mice. *Front*
912 *Immunol.* 2018;9:1092.

913 82. Klein L, Kyewski B, Allen PM, Hogquist KA. Positive and negative selection of the T cell
914 repertoire: what thymocytes see (and don't see). *Nat Rev Immunol.* 2014;14(6):377-91.

915 83. Caron E, Vincent K, Fortier MH, Laverdure JP, Bramoullé A, Hardy MP, et al. The MHC I
916 immunopeptidome conveys to the cell surface an integrative view of cellular regulation. *Mol Syst Biol.*
917 2011;7:533.

918 84. Admon A. The biogenesis of the immunopeptidome. *Semin Immunol.* 2023;67:101766.

919 85. Laumont CM, Vincent K, Hesnard L, Audemard E, Bonneil E, Laverdure JP, et al. Noncoding
920 regions are the main source of targetable tumor-specific antigens. *Sci Transl Med.* 2018;10(470).

921 86. Burbage M, Rocanin-Arjo A, Baudon B, Arribas YA, Merlotti A, Rookhuizen DC, et al.
922 Epigenetically controlled tumor antigens derived from splice junctions between exons and transposable
923 elements. *Sci Immunol.* 2023;8(80):eabm6360.

924 87. Shah NM, Jang HJ, Liang Y, Maeng JH, Tzeng SC, Wu A, et al. Pan-cancer analysis identifies
925 tumor-specific antigens derived from transposable elements. *Nat Genet.* 2023;55(4):631-9.

926 88. Shao W, Pedrioli PGA, Wolski W, Scurtescu C, Schmid E, Vizcaino JA, et al. The SysteMHC
927 Atlas project. *Nucleic Acids Res.* 2018;46(D1):D1237-D47.

928 89. Weijer K, Uittenbogaart CH, Voordouw A, Couwenberg F, Seppen J, Blom B, et al. Intrathymic
929 and extrathymic development of human plasmacytoid dendritic cell precursors in vivo. *Blood.*
930 2002;99(8):2752-9.

931 90. Boehm T, Morimoto R, Trancoso I, Aleksandrova N. Genetic conflicts and the origin of
932 self/nonself-discrimination in the vertebrate immune system. *Trends Immunol.* 2023;44(5):372-83.

933 91. Harroud A, Hafler DA. Common genetic factors among autoimmune diseases. *Science.*
934 2023;380(6644):485-90.

935 92. Bray NL, Pimentel H, Melsted P, Pachter L. Near-optimal probabilistic RNA-seq quantification.
936 *Nat Biotechnol.* 2016;34(5):525-7.

937 93. Smit A, Hubley, R & Green, P. RepeatMasker Open-4.0. 2013-2015.

938 94. Melsted P, Booeshaghi AS, Gao F, Beltrame E, Lu L, Hjorleifsson KE, et al. Modular and
939 efficient preprocessing of single-cell RNA-seq. *bioRxiv.* 2019:673285.

940 95. Langmead B, Salzberg SL. Fast gapped-read alignment with Bowtie 2. *Nat Methods.*
941 2012;9(4):357-9.

942 96. Danecek P, Bonfield JK, Liddle J, Marshall J, Ohan V, Pollard MO, et al. Twelve years of
943 SAMtools and BCFtools. *Gigascience.* 2021;10(2).

944 97. Zhang Y, Liu T, Meyer CA, Eeckhoute J, Johnson DS, Bernstein BE, et al. Model-based analysis
945 of ChIP-Seq (MACS). *Genome Biol.* 2008;9(9):R137.

946 98. Amemiya HM, Kundaje A, Boyle AP. The ENCODE Blacklist: Identification of Problematic
947 Regions of the Genome. *Sci Rep.* 2019;9(1):9354.

948 99. Quinlan AR, Hall IM. BEDTools: a flexible suite of utilities for comparing genomic features.
949 *Bioinformatics.* 2010;26(6):841-2.

950 100. Ramirez F, Ryan DP, Gruning B, Bhardwaj V, Kilpert F, Richter AS, et al. deepTools2: a next
951 generation web server for deep-sequencing data analysis. *Nucleic Acids Res.* 2016;44(W1):W160-5.

952 101. Kent WJ, Sugnet CW, Furey TS, Roskin KM, Pringle TH, Zahler AM, et al. The human genome
953 browser at UCSC. *Genome Res.* 2002;12(6):996-1006.

954 102. Shen L, Shao N, Liu X, Nestler E. ngs.plot: Quick mining and visualization of next-generation
955 sequencing data by integrating genomic databases. *BMC Genomics.* 2014;15:284.

956 103. Amezquita RA, Lun ATL, Becht E, Carey VJ, Carpp LN, Geistlinger L, et al. Orchestrating
957 single-cell analysis with Bioconductor. *Nat Methods*. 2020;17(2):137-45.

958 104. McCarthy DJ, Campbell KR, Lun AT, Wills QF. Scater: preprocessing, quality control,
959 normalization and visualization of single-cell RNA-seq data in R. *Bioinformatics*. 2017;33(8):1179-86.

960 105. Lun AT, McCarthy DJ, Marioni JC. A step-by-step workflow for low-level analysis of single-
961 cell RNA-seq data with Bioconductor. *F1000Res*. 2016;5:2122.

962 106. Haghverdi L, Lun ATL, Morgan MD, Marioni JC. Batch effects in single-cell RNA-sequencing
963 data are corrected by matching mutual nearest neighbors. *Nat Biotechnol*. 2018;36(5):421-7.

964 107. Gu Z, Gu L, Eils R, Schlesner M, Brors B. circlize Implements and enhances circular
965 visualization in R. *Bioinformatics*. 2014;30(19):2811-2.

966 108. Cowan JE, Malin J, Zhao Y, Seedhom MO, Harly C, Ohigashi I, et al. Myc controls a distinct
967 transcriptional program in fetal thymic epithelial cells that determines thymus growth. *Nat Commun*.
968 2019;10(1):5498.

969 109. Kowalczyk MS, Tirosh I, Heckl D, Rao TN, Dixit A, Haas BJ, et al. Single-cell RNA-seq reveals
970 changes in cell cycle and differentiation programs upon aging of hematopoietic stem cells. *Genome Res*.
971 2015;25(12):1860-72.

972 110. Lander ES, Linton LM, Birren B, Nusbaum C, Zody MC, Baldwin J, et al. Initial sequencing and
973 analysis of the human genome. *Nature*. 2001;409(6822):860-921.

974 111. Mouse Genome Sequencing C, Waterston RH, Lindblad-Toh K, Birney E, Rogers J, Abril JF, et
975 al. Initial sequencing and comparative analysis of the mouse genome. *Nature*. 2002;420(6915):520-62.

976 112. Lambert SA, Jolma A, Campitelli LF, Das PK, Yin Y, Albu M, et al. The Human Transcription
977 Factors. *Cell*. 2018;172(4):650-65.

978 113. Grant CE, Bailey TL, Noble WS. FIMO: scanning for occurrences of a given motif.
979 *Bioinformatics*. 2011;27(7):1017-8.

980 114. Butts CT. network: A Package for Managing Relational Data in R. *Journal of Statistical
981 Software*. 2008;24(2):1 - 36.

982 115. Abugessaisa I, Noguchi S, Hasegawa A, Kondo A, Kawaji H, Carninci P, et al. refTSS: A
983 Reference Data Set for Human and Mouse Transcription Start Sites. *J Mol Biol*. 2019;431(13):2407-22.

984 116. Oksanen J, Blanchet FG, Friendly M, Kindt R, Legendre P, McGlinn D, et al. vegan: Community
985 Ecology Package. 2020;<https://CRAN.R-project.org/package=vegan>.

986 117. Satija R, Farrell JA, Gennert D, Schier AF, Regev A. Spatial reconstruction of single-cell gene
987 expression data. *Nat Biotechnol*. 2015;33(5):495-502.

988 118. Baran Y, Bercovich A, Sebe-Pedros A, Lubling Y, Giladi A, Chomsky E, et al. MetaCell:
989 analysis of single-cell RNA-seq data using K-nn graph partitions. *Genome Biol*. 2019;20(1):206.

990 119. Stoeckle C, Rota IA, Tolosa E, Haller C, Melms A, Adamopoulou E. Isolation of myeloid
991 dendritic cells and epithelial cells from human thymus. *J Vis Exp*. 2013(79):e50951.

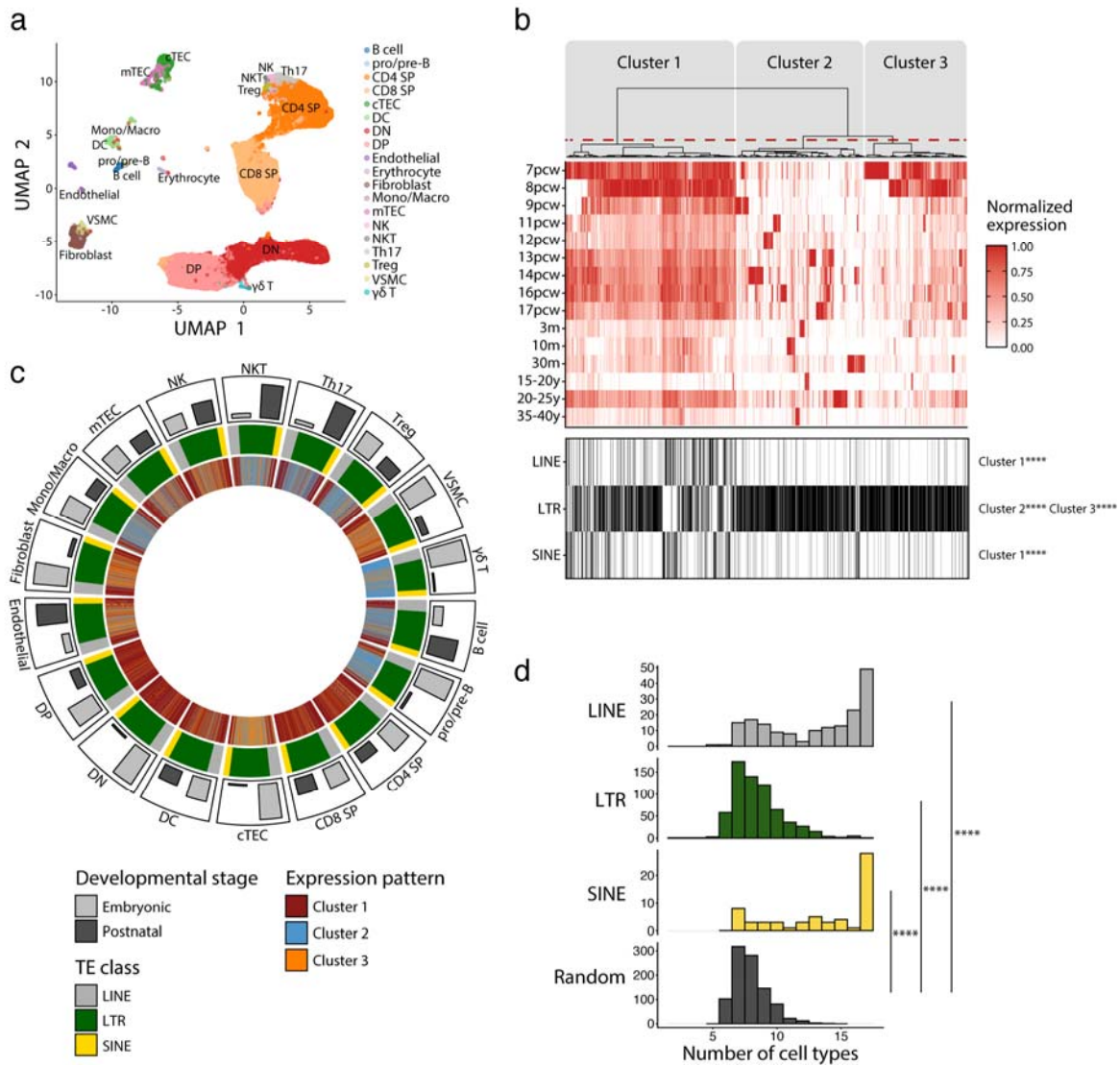
992 120. Ma Y, Sun S, Shang X, Keller ET, Chen M, Zhou X. Integrative differential expression and gene
993 set enrichment analysis using summary statistics for scRNA-seq studies. *Nat Commun*.
994 2020;11(1):1585.

995 121. Law CW, Chen Y, Shi W, Smyth GK. voom: Precision weights unlock linear model analysis
996 tools for RNA-seq read counts. *Genome Biol*. 2014;15(2):R29.

997 122. Ritchie ME, Phipson B, Wu D, Hu Y, Law CW, Shi W, et al. limma powers differential
998 expression analyses for RNA-sequencing and microarray studies. *Nucleic Acids Res*. 2015;43(7):e47.

999 123. Broseus L, Ritchie W. S-IRFindeR: stable and accurate measurement of intron retention.
1000 bioRxiv. 2020;2020.06.25.164699.

1001 124. Dobin A, Davis CA, Schlesinger F, Drenkow J, Zaleski C, Jha S, et al. STAR: ultrafast universal
1002 RNA-seq aligner. Bioinformatics. 2013;29(1):15-21.
1003 125. Kim MJ, Miller CM, Shadrach JL, Wagers AJ, Serwold T. Young, proliferative thymic epithelial
1004 cells engraft and function in aging thymuses. J Immunol. 2015;194(10):4784-95.
1005

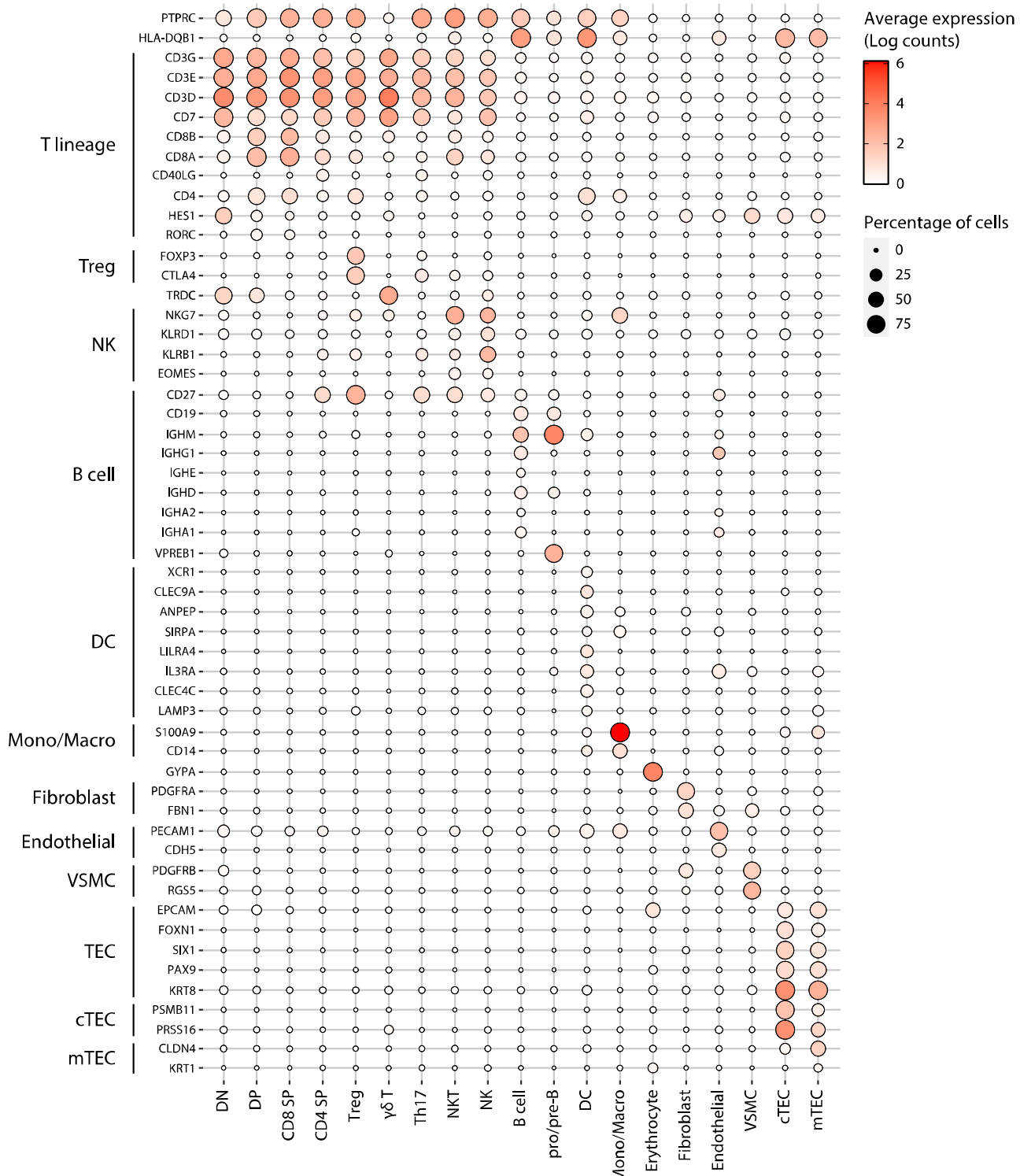


1006

1007 **Figure 1. LINEs, SINEs, and LTRs exhibit distinct expression profiles in human thymic cell**
1008 **populations. (a)** UMAP depicting the cell populations present in human thymus (CD4 SP, CD4 single
1009 positive thymocytes; CD8 SP, CD8 single positive thymocytes; cTEC, cortical thymic epithelial cells;
1010 DC, dendritic cells; DN, double negative thymocytes; DP, double positive thymocytes; Mono/Macro,

1011 monocytes and macrophages; mTEC, medullary thymic epithelial cells; NK, natural killer cells; NKT,
1012 natural killer T cells; pro/pre-B, pro-B and pre-B cells; Th17, T helper 17 cells; Treg, regulatory T cells;
1013 VSMC, vascular smooth muscle cell). Cells were clustered in 19 populations based on the expression of
1014 marker genes from *Park et al.* (40). **(b)** *Upper panel*: Heatmap of TE expression during thymic
1015 development, with each column representing the expression of one TE subfamily in one cell type.
1016 Unsupervised hierarchical clustering was performed, and the dendrogram was manually cut into 3
1017 clusters (red dashed line). *Lower panel*: The class of TE subfamilies and significant enrichments in the 3
1018 clusters (Fisher's exact tests; ****p≤0.0001). (pcw, post-conception week; m, month; y, year). **(c)**
1019 Circos plot showing the expression pattern of TE subfamilies across thymic cells. From outermost to
1020 innermost tracks: i) proportion of cells in embryonic and postnatal samples, ii) class of TE subfamilies,
1021 iii) expression pattern of TE subfamilies identified in (b). TE subfamilies are in the same order for all
1022 cell types. **(d)** Histograms showing the number of cell types sharing the same expression pattern for a
1023 given TE subfamily. LINE (n=171), LTR (n=577), and SINE (n=60) were compared to a randomly
1024 generated distribution (n=809) (Kolmogorov-Smirnov tests, ****p≤0.0001).

1025

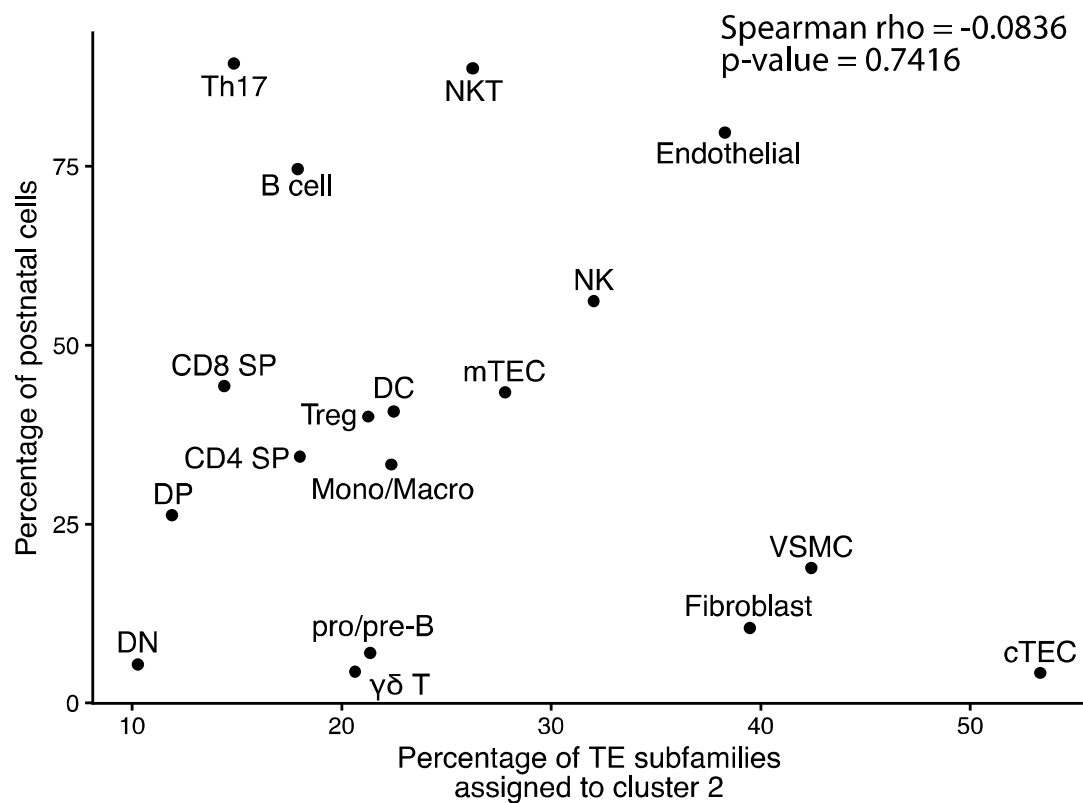


1026

1027 **Figure 1 – figure supplement 1. Annotation of human thymic cell populations.**

1028 Dot plot depicting the expression of marker genes in the annotated cell types of the thymus. The average
1029 expression and percentage of cells expressing the gene are represented by the color and size of the dot,
1030 respectively (DN, double negative thymocytes; DP, double positive thymocytes; CD8 SP, CD8 single
1031 positive thymocytes; CD4 SP, CD4 single positive thymocytes, Treg, regulatory T cells; NKT, natural
1032 killer T cells; NK, natural killer cells; DC, dendritic cells; Mono/Macro, monocytes and macrophages;
1033 VSMC, vascular smooth muscle cells; cTEC, cortical thymic epithelial cells; mTEC, medullary thymic
1034 epithelial cells).

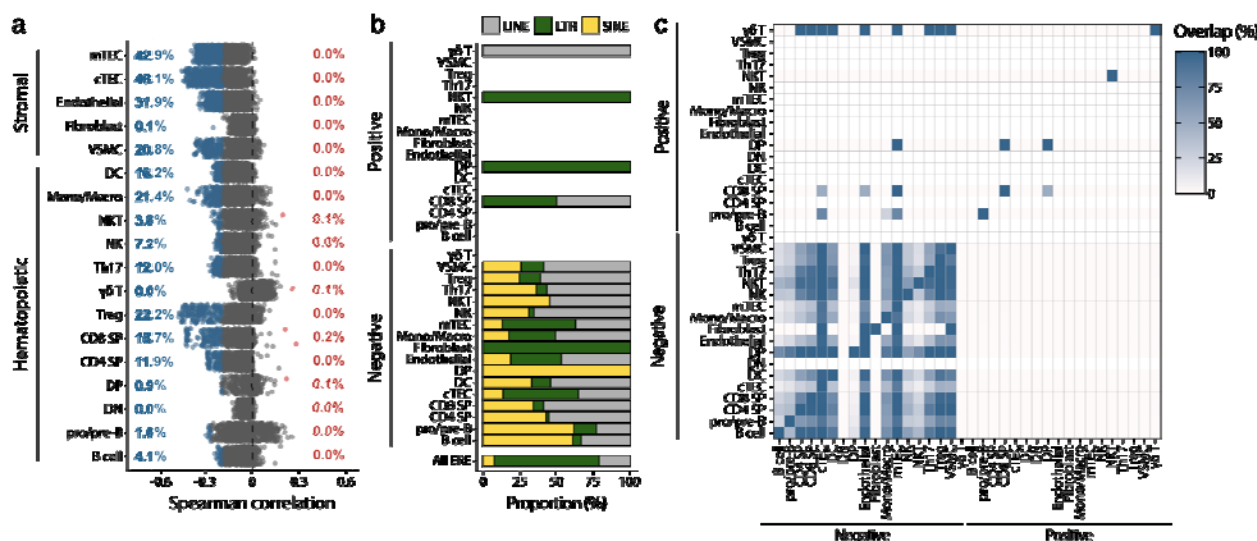
1035



1036

1037 **Figure 1 – figure supplement 2. Assignment to cluster 2 is independent of the developmental stage
1038 of cells.**

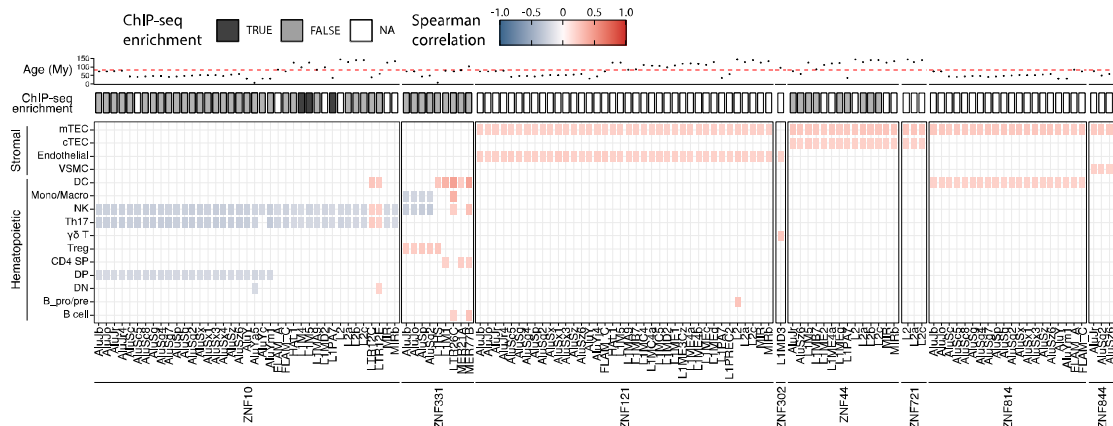
1039 The graph depicts the correlation between the proportion of cells of a population originating from a
1040 postnatal sample and the proportion of TE subfamilies assigned to cluster 2 by the hierarchical
1041 clustering in Figure 1B.



1042

1043 **Figure 1 – figure supplement 3. TE expression is negatively correlated with cell proliferation.**

1044 (a) Spearman correlation between the expression of TE subfamilies and cell cycle scores. Positively
 1045 ($r \geq 0.2$ and adj. $p \leq 0.01$) and negatively ($r \leq -0.2$ and adj. $p \leq 0.01$) correlated subfamilies are red and blue,
 1046 respectively. P-values were corrected for multiple comparisons with the Benjamini-Hochberg method).
 1047 (b) Proportion of subfamilies positively or negatively correlated with cell proliferation belonging to each
 1048 TE class. (c) Percentage of overlap of TE subfamilies positively or negatively correlated with cell
 1049 proliferation between cell types.

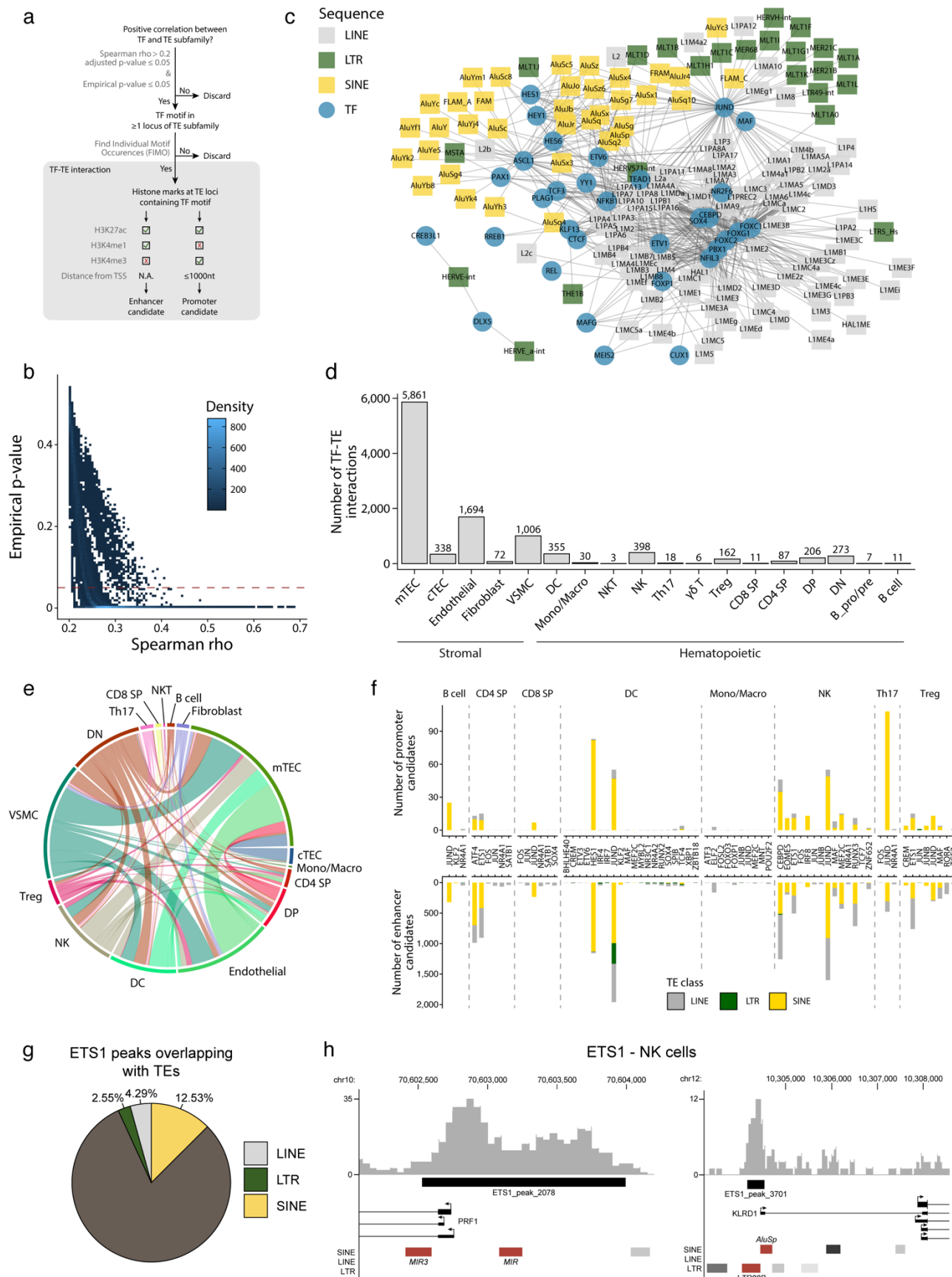


1050

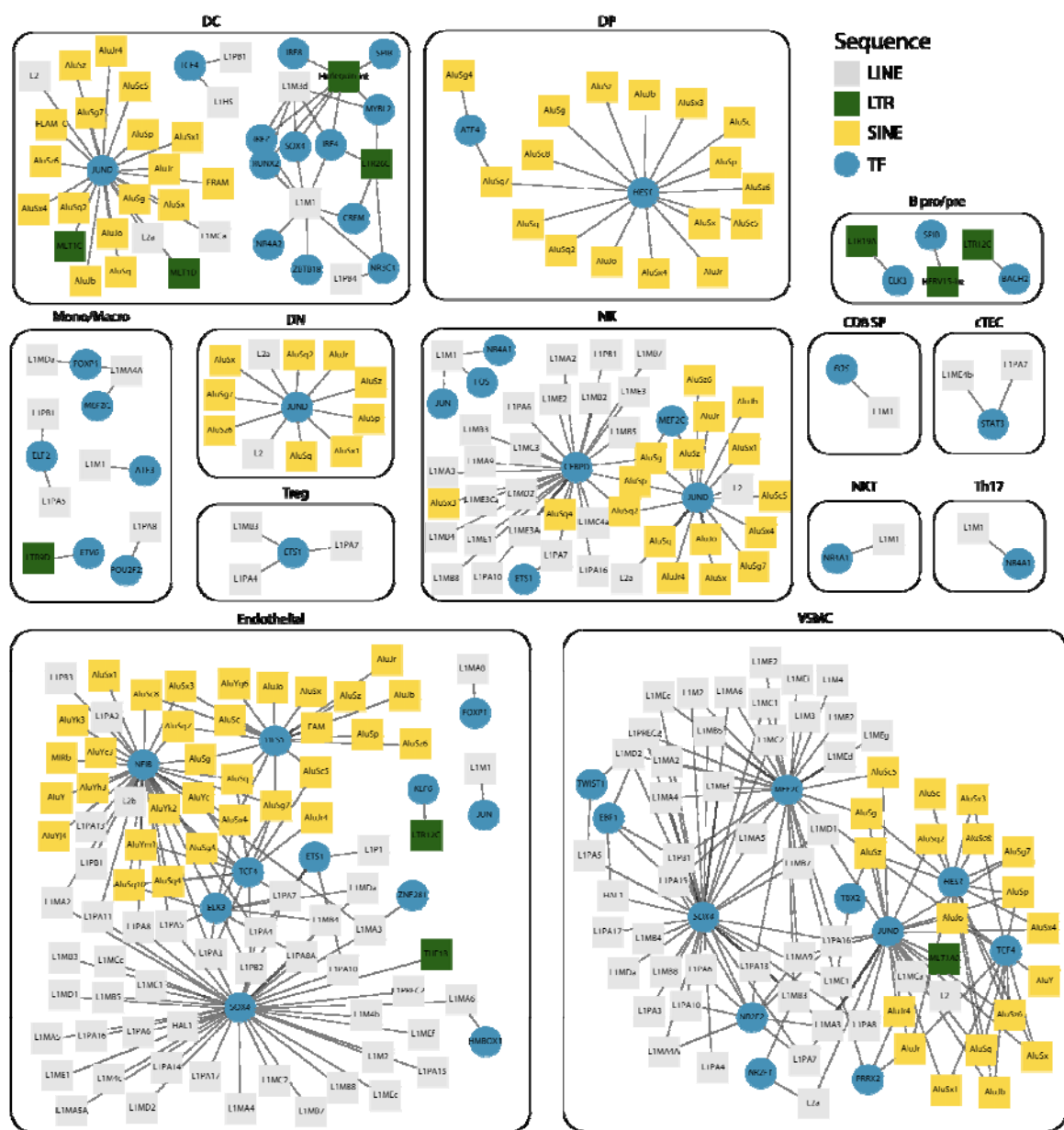
1051 **Figure 1 – figure supplement 4. KZFPs repress TE expression in the hematopoietic lineage of the**
1052 **human thymus.**

1053 *Lower panel:* pairs of TE subfamilies and KZFPs significantly correlated in at least two cell types
1054 (significant correlation: $r>0.2$ and adj. $p\leq0.05$, or $r<-0.2$ and adj. $p\leq0.05$, p-values corrected for multiple
1055 comparisons with the Benjamini-Hochberg method). *Middle panel:* Enrichment of the KZFP in the
1056 sequence of the correlated TE subfamily in ChIP-seq data from *Imbeault et al.* (44). *Upper panel:* Age
1057 of TE subfamilies in millions of years (My). The dashed line indicates the estimated time of divergence
1058 between primates and rodents (82 million years ago).

1059

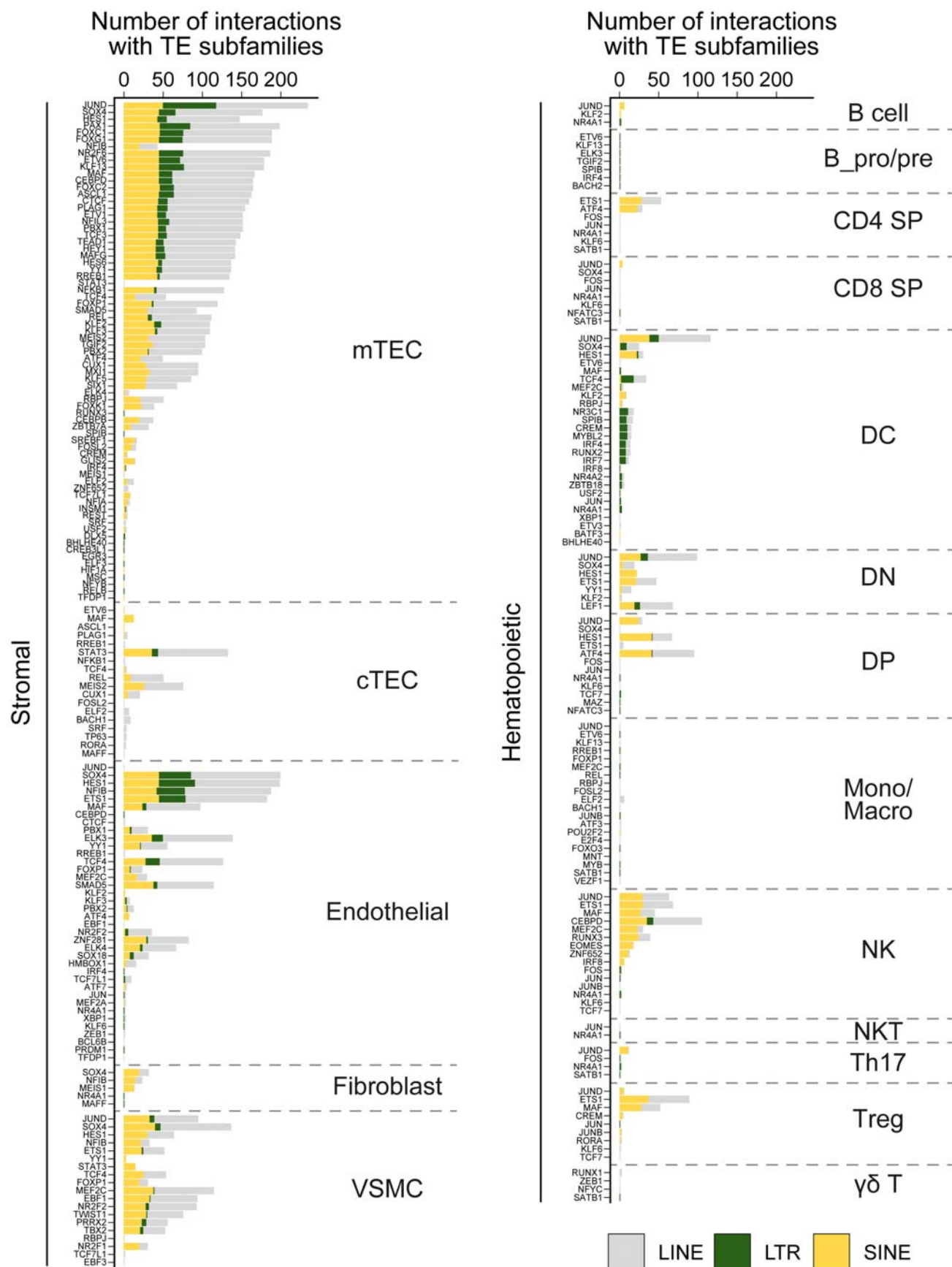


1061 **Figure 2. TEs shape complex gene regulatory networks in human thymic cells.** (a) The flowchart
1062 depicts the decision tree for each TE promoter or enhancer candidate. (b) Density heatmap representing
1063 the correlation coefficient and the empirical p-value determined by bootstrap for TF and TE pairs in
1064 each cell type of the dataset. The color code shows density (i.e., the occurrence of TF-TE pairs at a
1065 specific point). (c) Connectivity map of interactions between TEs and TFs in mTECs. For visualization
1066 purposes, only TF-TE pairs with high positive correlations (Spearman correlation coefficient ≥ 0.3 and
1067 p-value adjusted for multiple comparisons with the Benjamini-Hochberg procedure ≤ 0.05) and TF
1068 binding sites in $\geq 1\%$ of TE loci are shown. (d) Number of TF-TE interactions for each thymic cell
1069 population. (e) Sharing of TF-TE pairs between thymic cell types. (f) Number of promoter (*top*) or
1070 enhancer (*bottom*) TE candidates per transcription factor in hematopoietic cells of the thymus. (g) The
1071 proportion of statistically significant peaks overlapping with TE sequences in ETS1 ChIP-seq data from
1072 NK cells. (h) Genomic tracks depicting the colocalization of ETS1 occupancy (i.e., read coverage) and
1073 TE sequences (*in red*) in the upstream region of two genes in ETS1 ChIP-seq data from NK cells.
1074 Statistically significant ETS1 peaks are indicated by the black rectangles.



1076 **Figure 2 – figure supplement 1. Interaction networks between transcription factors and TE**
1077 **subfamilies.**

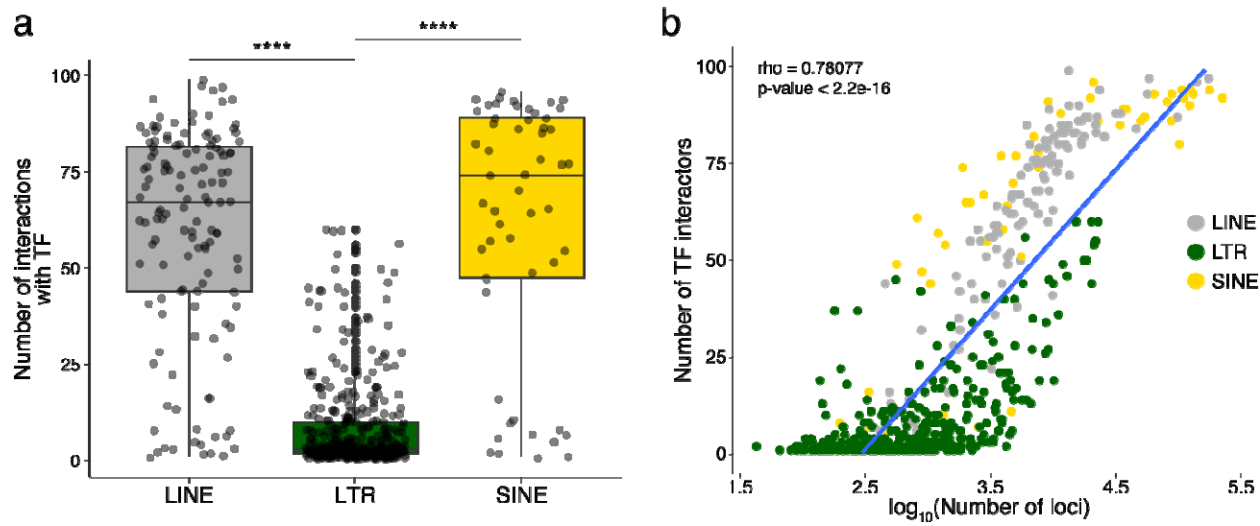
1078 For each cell type, networks illustrate the interactions between TF and TE subfamilies. Pairs of TF and
1079 TE are connected by edges when i) their expressions are significantly correlated (Spearman correlation
1080 coefficient ≥ 0.2) and ii) the TF binding motifs are found in the loci of the TE subfamily. TE subfamilies
1081 are colored based on the class of TE subfamily (LINE, LTR, and SINE).



1083 **Figure 2 – figure supplement 2. Frequency of interactions between transcription factors and TE**
1084 **subfamilies in thymic cells.** For each cell type of the stromal (*left*) or hematopoietic (*right*)
1085 compartments of the thymus, the graph shows the number of interactions between transcription factors
1086 and TE subfamilies of the LINE, LTR, or SINE groups.

1087

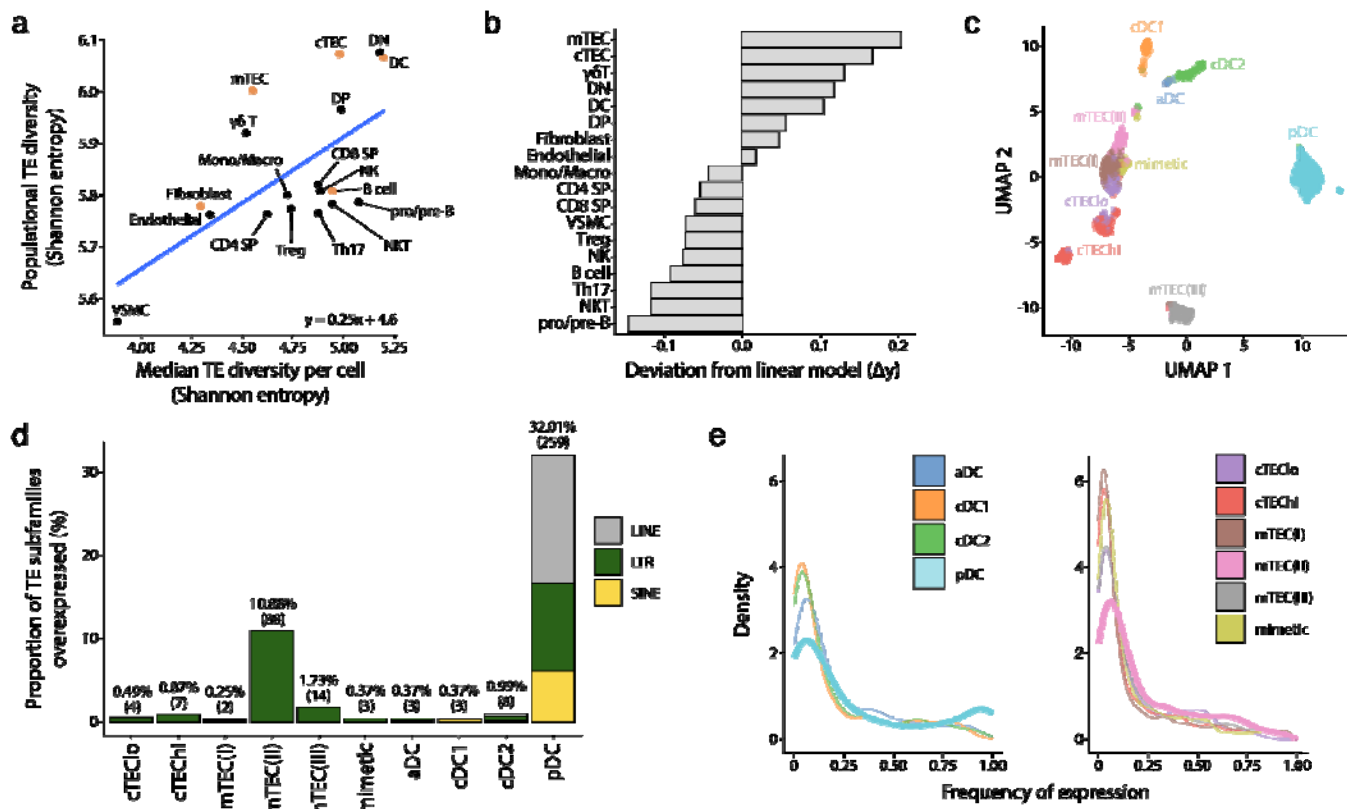
1088



1089

1090 **Figure 2 – figure supplement 3. TE subfamilies occupying larger genomic spaces interact more**
1091 **frequently with TF.**

1092 (a) Number of interactions formed with TFs for each TE subfamily of the LINE, LTR, and SINE classes
1093 (Wilcoxon-Mann-Whitney tests, **** $p \leq 0.0001$). (b) Scatterplot depicting the Kendall tau correlation
1094 between the number of interactions with TFs of a TE subfamily and the number of loci of that subfamily
1095 in the human genome. The color code indicates the class of TE subfamilies.

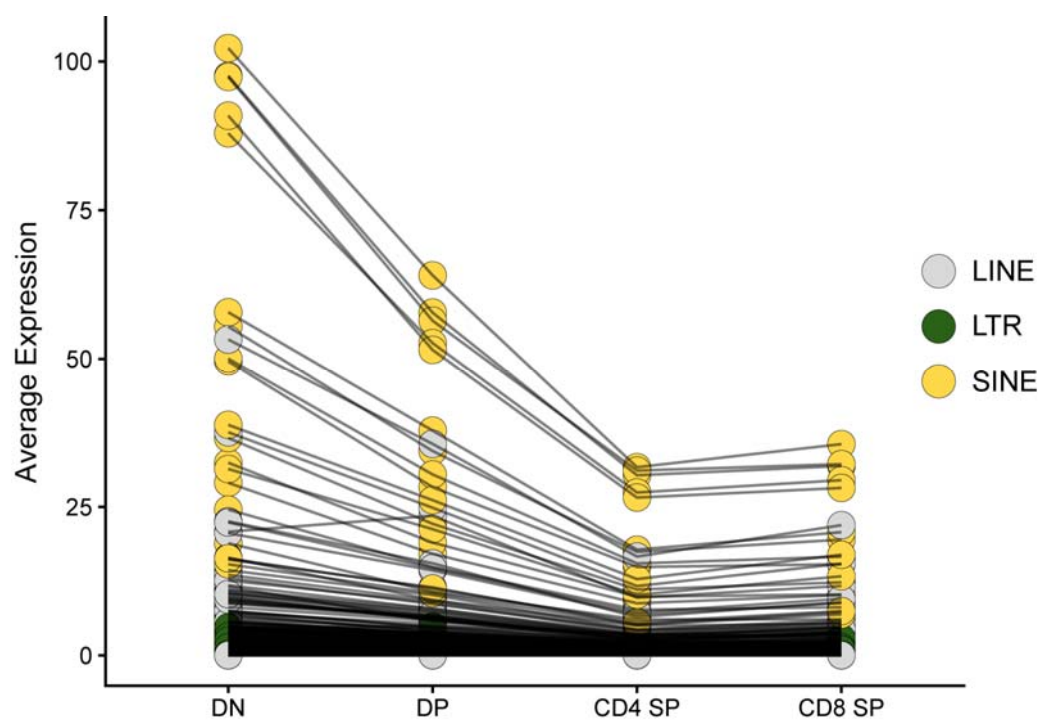


1096

1097 **Figure 3. Human pDCs and mTEC(II) express diverse and distinct repertoires of TE sequences.**

1098 **(a)** Diversity of TEs expressed by thymic populations measured by Shannon entropy. The x and y axes
 1099 represent the median diversity of TEs expressed by individual cells in a population and the global
 1100 diversity of TEs expressed by an entire population, respectively. The equation and blue curve represent a
 1101 linear model summarizing the data. Thymic APC subsets are indicated in orange. **(b)** Difference
 1102 between the observed diversity of TEs expressed by cell populations and the one expected by the linear
 1103 model in (A). **(c)** UMAP showing the subsets of thymic APCs (aDC, activated DC; cDC1, conventional
 1104 DC1; cDC2, conventional DC2; pDC, plasmacytoid DC). **(d)** Bar plot showing the number and class of
 1105 differentially expressed TE subfamilies between APC subsets. **(e)** Frequency of expression of TE
 1106 subfamilies by the different APC subsets. The distributions for pDCs and mTEC(II) are highlighted in
 1107 bold.

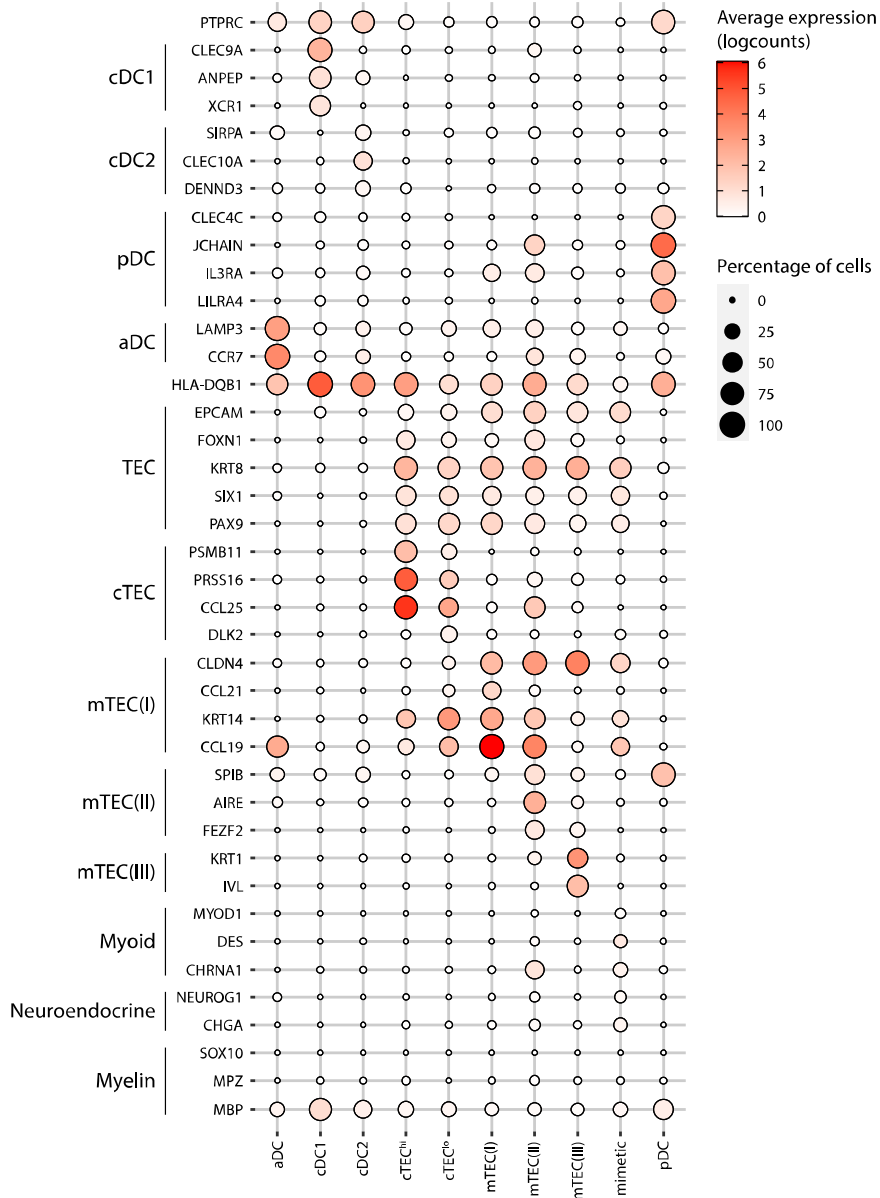
1108



1109

1110 **Figure 3 – figure supplement 1. TE expression decreases during thymocyte differentiation.** The
1111 average expression level of TE subfamilies across cells of the four main populations of thymocytes is
1112 shown: DN, DP, CD4 SP, and CD8 SP. Black lines between thymocyte subsets connect expression
1113 values for the same TE subfamily.

1114



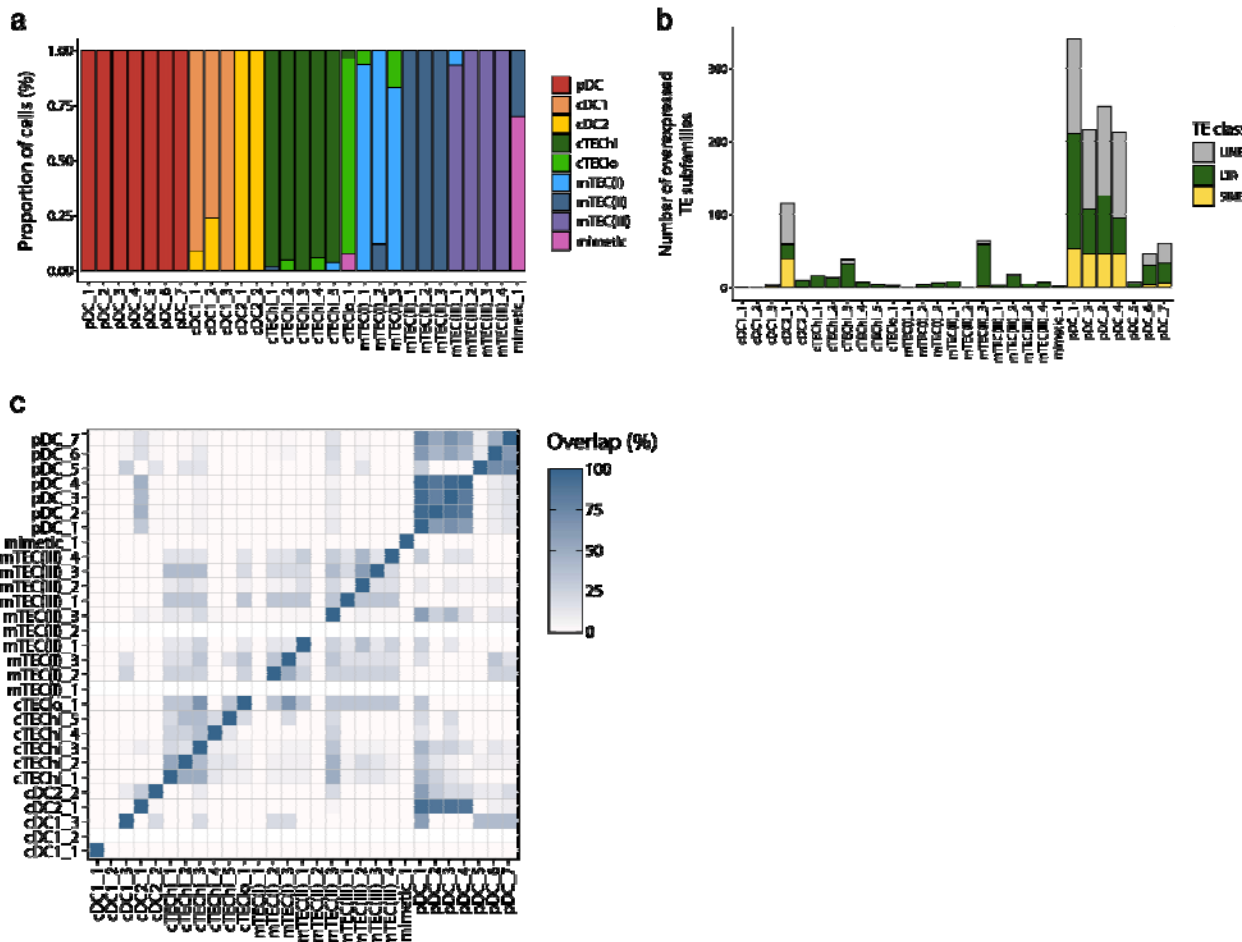
1115

1116 **Figure 3 – figure supplement 2. Annotation of human thymic antigen-presenting cell subsets.**

1117 Dot plot depicting the expression of marker genes in the annotated cell types of the thymus. The average
 1118 expression and percentage of cells expressing the gene are represented by the color and size of the dot,
 1119 respectively. Myoid-, myeloid- and neuroendocrine-related genes are used as markers of mimetic
 1120 mTEC. (aDC, activated dendritic cell; cDC1, conventional dendritic cell 1; cDC2, conventional

1121 dendritic cell 2; cTEC, cortical thymic epithelial cell; mTEC, medullary thymic epithelial cell; pDC,
1122 plasmacytoid dendritic cell).

1123



1124

1125 **Figure 3 – figure supplement 3. Differential TE expression in metacells of human thymic antigen-
1126 presenting cells.**

1127 (a) Cellular composition of the metacells (x-axis) based on the manual annotation of the thymic cell
1128 populations (see Fig. S1). (b) Number of TE subfamilies overexpressed expressed between the
1129 metacells. TE subfamilies are colored based on class (LINE, LTR, and SINE). (c) Percentage of overlap
1130 of the TE subfamilies overexpressed by each metacell.

1131

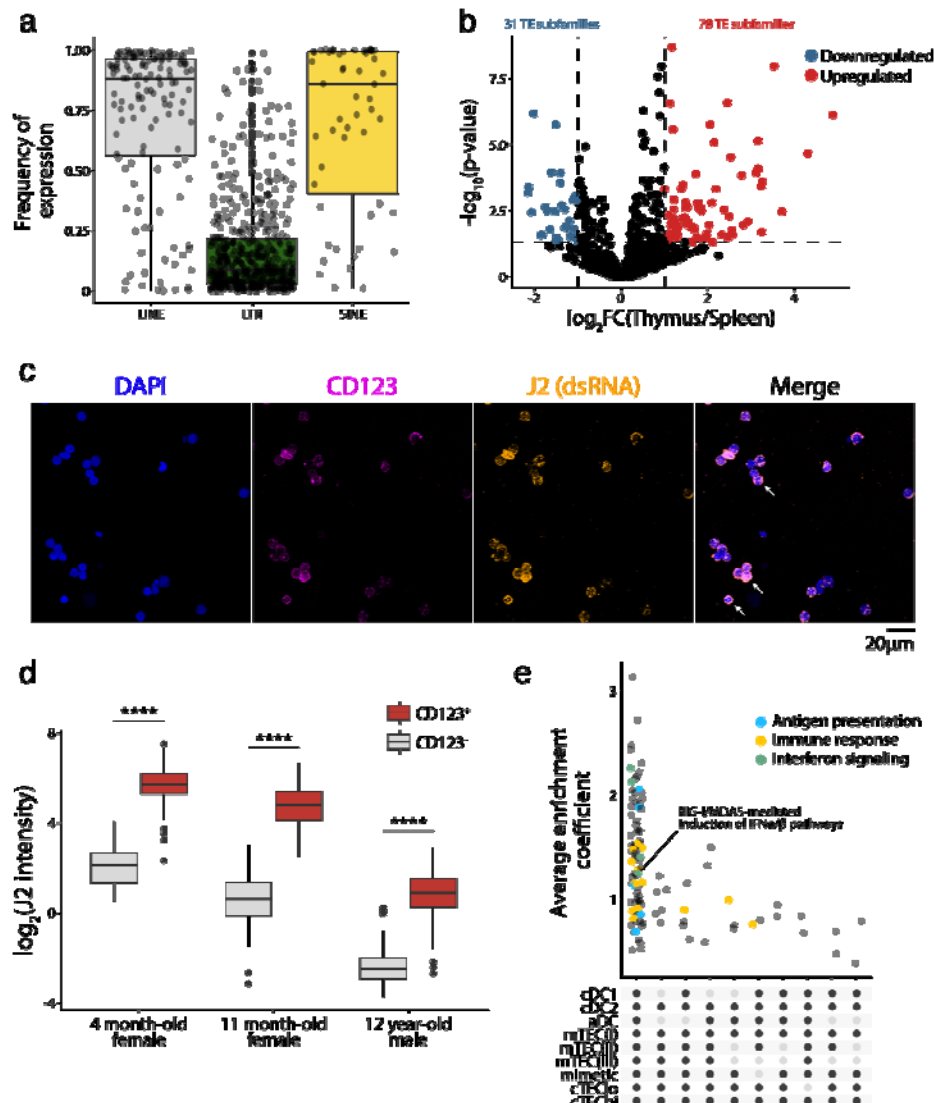
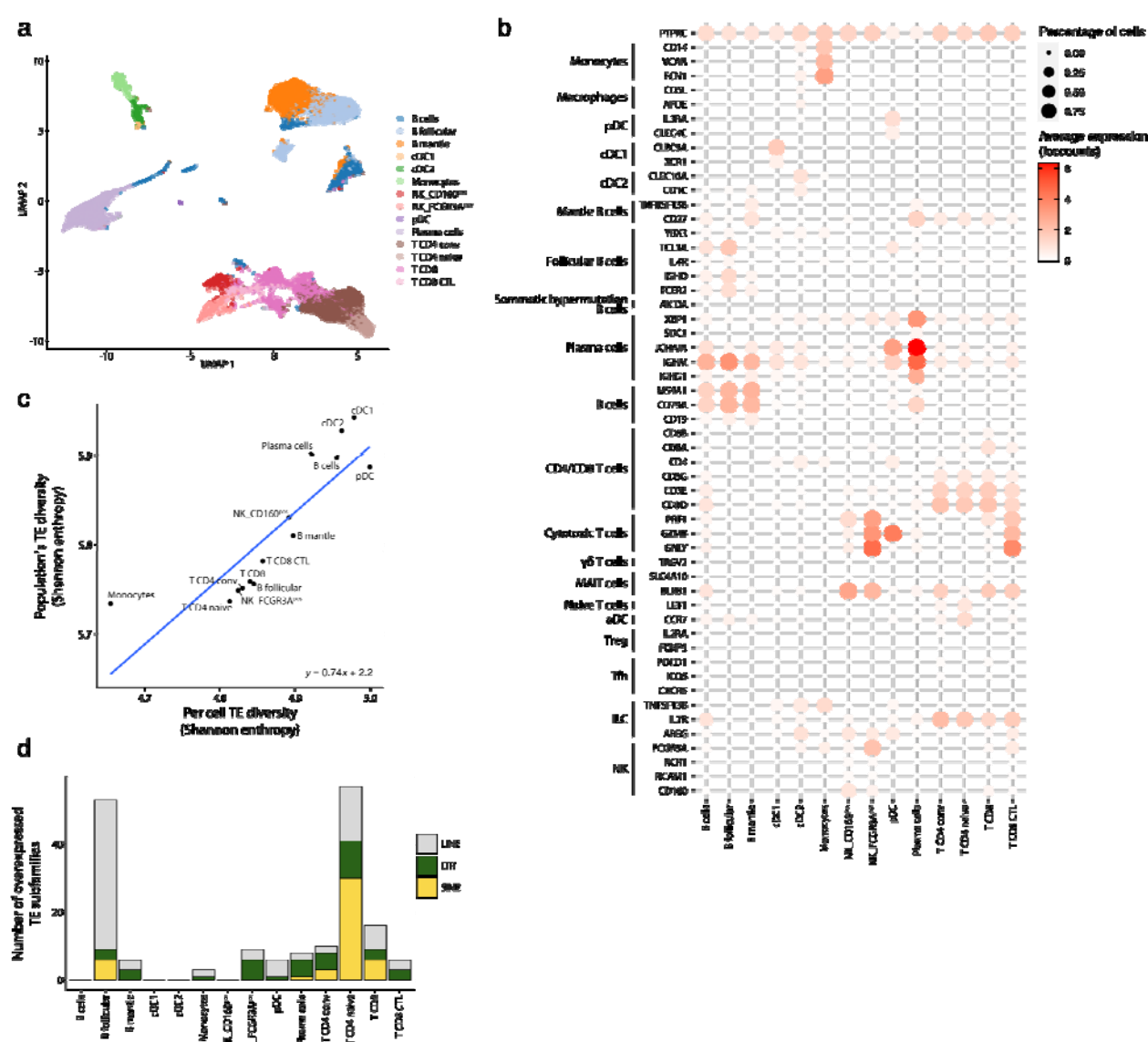


Figure 4. TE expression in human pDCs is associated with dsRNA formation and type I IFN signaling. (a) Frequency of LINE, LTR, and SINE subfamilies expression in thymic pDCs. (b) Differential expression of TE subfamilies between splenic and thymic pDCs. TE subfamilies significantly upregulated or downregulated by thymic pDCs are indicated in red and blue, respectively (Upregulated, $\log_2(\text{Thymus/Spleen}) \geq 1$ and adj. $p \leq 0.05$; Downregulated, $\log_2(\text{Thymus/Spleen}) \leq -1$ and adj. $p \leq 0.05$). (c,d) Immunostaining of dsRNAs in human thymic pDCs ($CD123^+$) using the J2 antibody ($n=3$). (c) One representative experiment. Three examples of $CD123$ and J2 colocalization are shown with white arrows. (d) J2 staining intensity in $CD123^+$ and $CD123^-$ cells from three human thymus.

1141 (Wilcoxon Rank Sum test, ****p-value≤0.0001). (e) UpSet plot showing gene sets enriched in pDCs
 1142 compared to the other populations of thymic APCs. On the lower panel, black dots represent cell
 1143 populations for which gene signatures are significantly depleted compared to pDCs. All comparisons
 1144 where gene signatures were significantly enriched in pDCs are shown.

1145

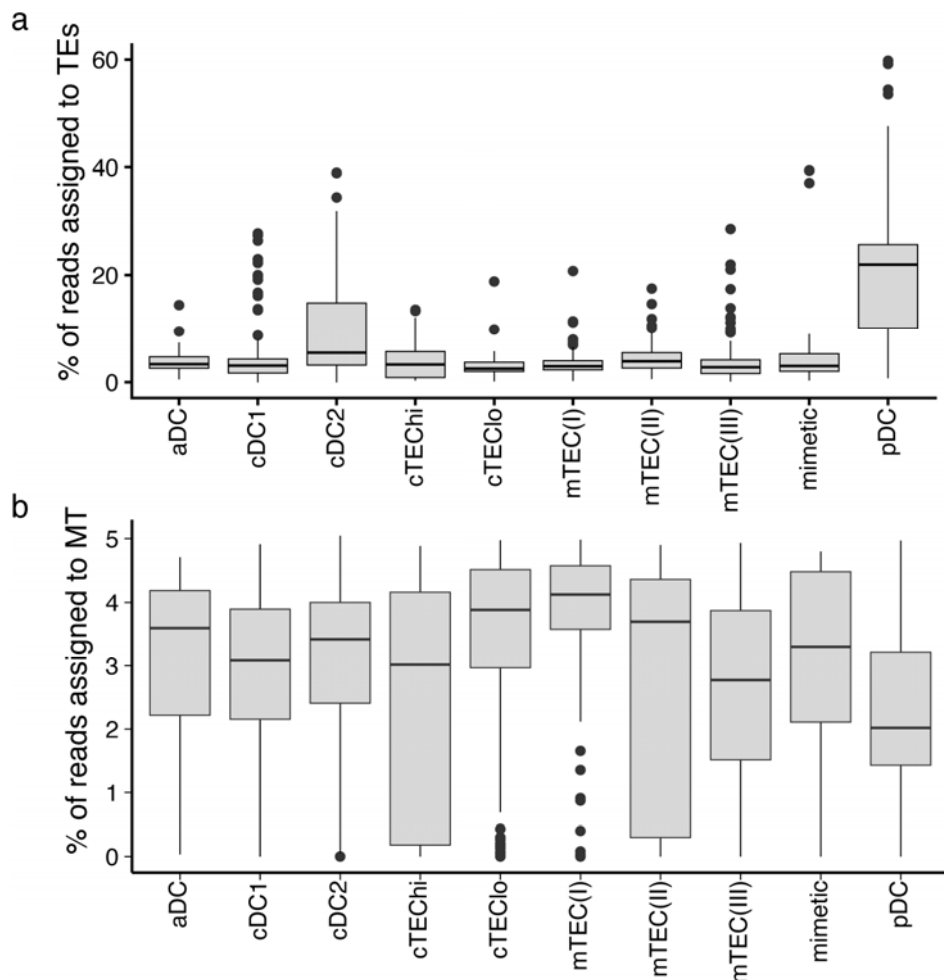


1146

1147 **Figure 4 – figure supplement 1. TE expression in human splenic pDCs.**

1148 (a) UMAP depicting the cell populations present in the human spleen. (b) Dot plot showing the
1149 expression of marker genes in the annotated cell types of the spleen. The average expression and
1150 percentage of cells expressing the gene are represented by the color and size of the dot, respectively. (c)
1151 Diversity of TE expressed by splenic populations measured by Shannon entropy. The x and y axes
1152 represent the median diversity of TE expressed by individual cells of a population and the global
1153 diversity of TE expressed by discrete populations, respectively. The equation and blue curve represent a
1154 linear model summarizing the data. (d) Bar plot showing the number (y-axis) and class (color) of
1155 differentially expressed TE subfamilies between splenic cell populations.

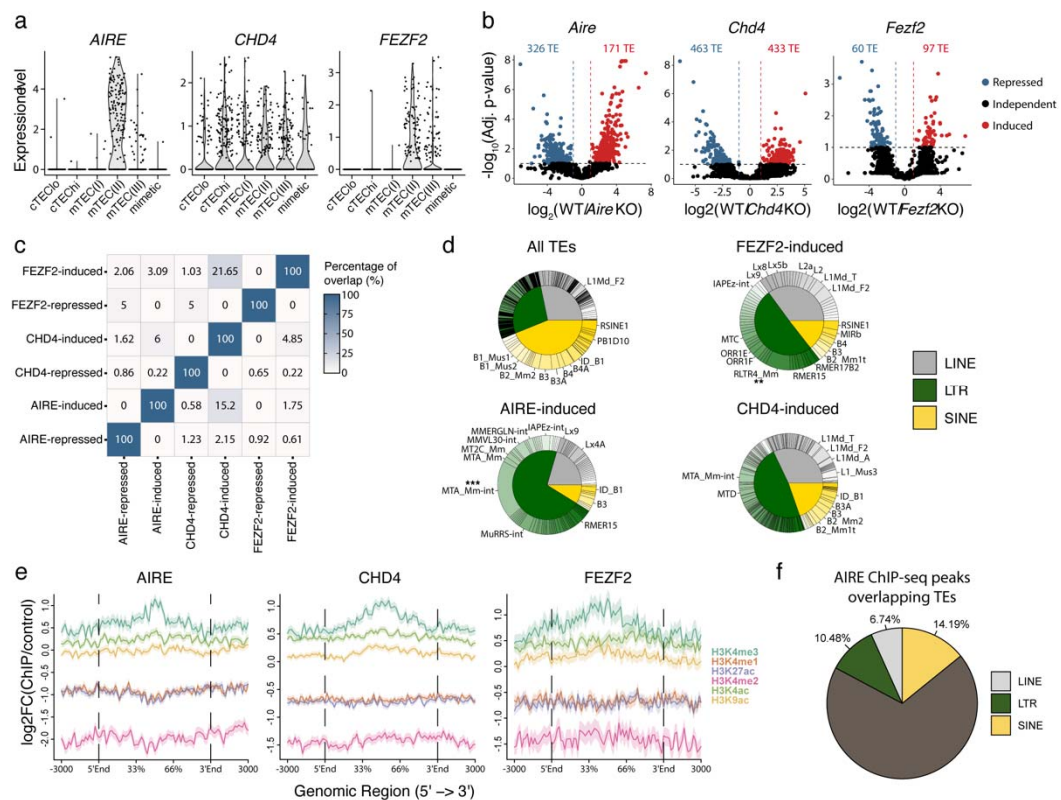
1156



1157

1158 **Figure 4 – figure supplement 2. A higher proportion of reads originates from TEs in pDCs than in**
 1159 **other thymic APCs.** Boxplots depicting the percentage of reads assigned to **(a)** TE sequences or **(b)**
 1160 mitochondrial reads in the different subpopulations of thymic APCs.

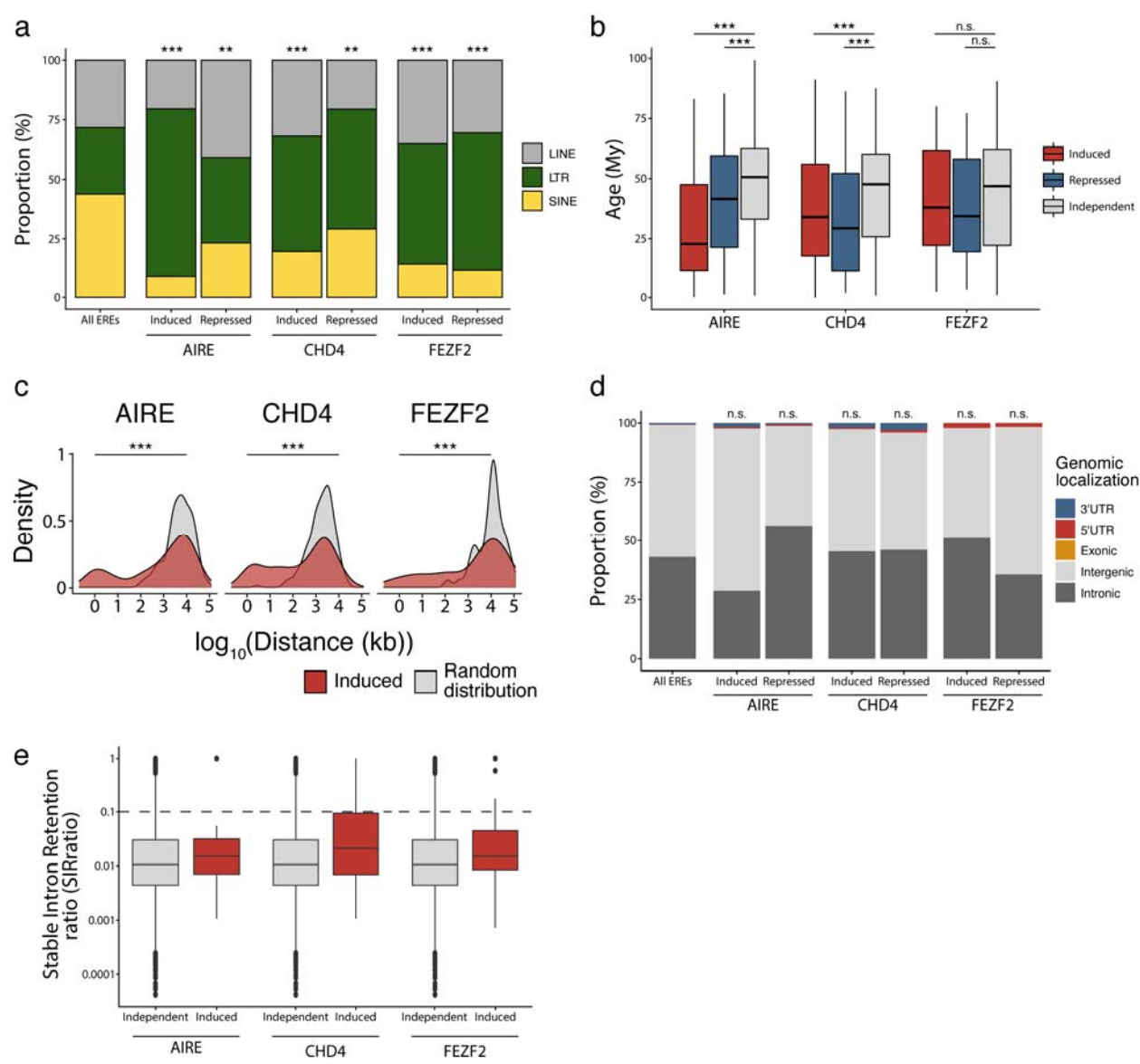
1161



1162

1163 **Figure 5. AIRE, FEZF2, and CHD4 regulate non-redundant sets of TEs in murine mTECs. (a)**
 1164 Expression of *AIRE*, *CHD4*, and *FEZF2* in human TEC subsets. **(b)** Differential expression of TE loci
 1165 between wild-type (WT) and *Aire*-, *Chd4*- or *Fezf2*-knockout (KO) mice (Induced, $\log_2(\text{WT}/\text{KO}) \geq 2$ and
 1166 adj. $p \leq 0.05$; Repressed, $\log_2(\text{WT}/\text{KO}) \leq -2$ and adj. $p \leq 0.05$). P-values were corrected for multiple
 1167 comparisons with the Benjamini-Hochberg procedure. The numbers of induced (red) and repressed
 1168 (blue) TE loci are indicated on the volcano plots. **(c)** Overlap of TE loci repressed or induced by *AIRE*,
 1169 *FEZF2*, and *CHD4*. **(d)** Proportion of TE classes and subfamilies in the TE loci regulated by *AIRE*,

1170 FEZF2, or CHD4, as well as all TE loci in the murine genome for comparison (Chi-squared tests with
 1171 Bonferroni correction, **adj. $p \leq 0.01$, ***adj. $p \leq 0.001$). (e) Plots for the tag density of H3K4me3 and
 1172 H3K4me2 on the sequence and flanking regions (3000 base pairs) of TE loci induced by AIRE, FEZF2,
 1173 and CHD4. (f) Proportion of statistically significant peaks overlapping TE sequences in AIRE ChIP-seq
 1174 data from murine mTECs.

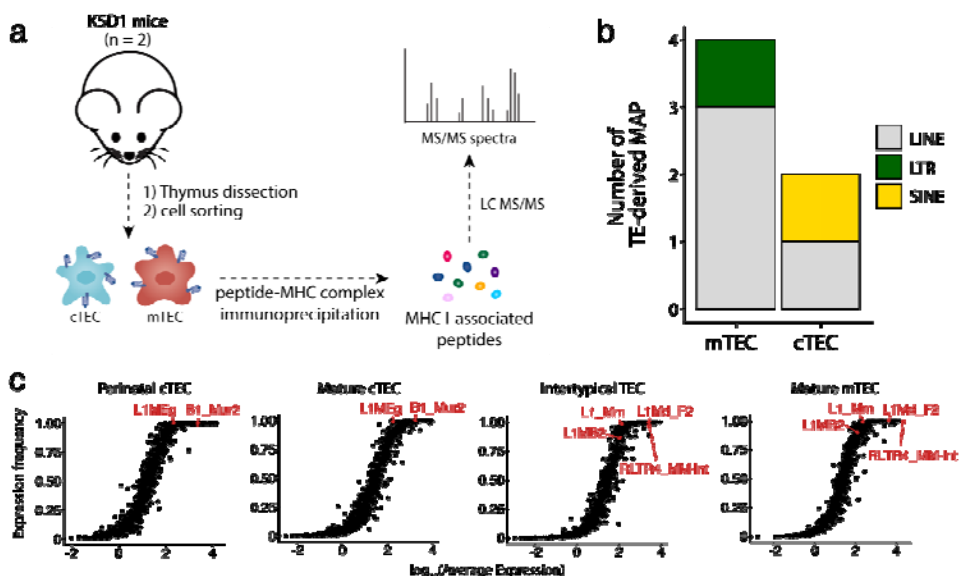


1175

1176 **Figure 5 – figure supplement 1. Characterization of TE subfamilies regulated by AIRE, CHD4,**
 1177 **and FEZF2 in murine mTECs.**

1178 (a) Class of TEs induced or repressed by AIRE, CHD4, and FEZF2. Distributions were compared to the
1179 proportion of LINEs, LTRs, and SINEs amongst all TE sequences of the murine genome with Chi-
1180 squared tests (**p≤0.01, ***p≤0.001). (b) Age of TEs induced, repressed, or independent of AIRE,
1181 CHD4, and FEZF2 (Wilcoxon-Mann-Whitney test, *p≤0.05, ***p≤0.001) (My, millions of years). (c)
1182 Distance between TE loci induced by AIRE, FEZF2, and CHD4, and random selections of TE loci
1183 (Wilcoxon rank-sum tests, ***p≤0.001). (d) Genomic localization of the TE loci induced or repressed
1184 by AIRE, CHD4, and FEZF2. (e) Intron retention ratio of intronic TE induced or independent of AIRE,
1185 CHD4, and FEZF2. The dashed line represents intron retention events occurring in at least 10% of
1186 transcripts.

1187



1188

1189 **Figure 6. Murine cTECs and mTECs present TE MAPs.** (a) mTECs and cTECs were isolated from
1190 the thymi of K5D1 mice (n=2). The peptide-MHC I complexes were immunoprecipitated independently
1191 for both populations, and MAPs were sequenced by MS analyses. (b) Number of LINE-, LTR-, and

1192 SINE-derived MAPs in mTECs and cTECs from K5D1 mice. **(c)** Distributions of TE subfamilies in
1193 murine TECs subsets based on expression level (*x-axis*) and frequency of expression (*y-axis*).